Delft University of Technology

Department of Materials Science and Engineering

Faculty of Mechanical, Maritime and Materials Engineering

Hydrogen absorption and conservation of operational capabilities in remanufactured bearing steel exposed to corrosion

A thesis submitted in partial fulfilment of the requirements for the degree of Master of Science in

Materials Science and Engineering

To be defended publically on 15th May 2023 at 09:00

Author:

Eider Barazar Garcia

5388619

Graduation Committee:

Dr. Erik Vegter (SKF supervisor)

Dr. Vera Popovich (supervisor)

Dr. Yaiza Gonzalez García (supervisor)

Dr. Amarante Bottger

Acknowledgements

Firstly, I would like to thank my supervisor from SKF, Erik Vegter, for giving me the opportunity to participate on this project, and the assistance in completing the work. Also thank my supervisors from TU Delft, Vera Popovich and Yaiza García Gonzalez, for their guidance and encouragement throughout this research.

I would like to extend my appreciation to all members at SKF Engineering and Research Centre in Houten for their guidance, and for providing the materials and facilities to carry out the laboratory work. Special thanks to Mohammed Faid for his constant input, scientific advise and discussions throughout the project.

Finally, my sincere appreciation to my family and friends for their encouragement and inspiration. Without them this accomplishment would not have been possible. Special thanks to mom, dad, Uzuri, Inma and grandma for their unwavering support and for always believing in me unconditionally.

Abstract

The corrosion of bearing steel often leads to accelerated damage and loss of properties that condition their service life. This damage is further exacerbated with the absorption of hydrogen into the material, generated from corrosion reactions happening at the surface. A remanufacturing process is proposed to recover the operating capabilities of bearings after exposure to corrosive environments, during which the bearings are polished until the surface is visually clean, out of any corrosion product. The process offers the recoverability of the operating capabilities and turns the corroded bearings into a reconditioned useful part avoiding the operational effort, economic cost, and repair that the replacement of a bearing entails. However, atomic hydrogen in the bulk can be entrapped and might still condition bearings operation, often resulting in hydrogen-enhanced damage in the steel.

The goal of the current research is to quantify the hydrogen uptake and criticaly evaluate the reapplication of such remanufactured bearings. The study analyses a bearing that experienced corrosion during its operation in the pulp and paper industry (P&P), primarily due to the cooling water used in the machines. For a better understanding of the effects of the operating environment on bearings, extreme corrosive environments were simulated in a Climate corrosion chamber (CCC). The absorbed bulk hydrogen is quantified through the Melt extraction tester (MET), and the trapping behaviour analysed through Thermal Desorption Spectrometry (TDS). The effect of the environmental conditions is studied through a microscopical characterization of the formed corrosion product. Optical Microscopy (OM), Scanning Electron Microscopy (SEM), Energy Dispersive X-ray Spectroscopy (EDS), X-ray Photoelectron Spectroscopy (XPS) are the laboratory equipment used for this purpose.

It was found that the remanufacturing did not ensure meeting the acceptable hydrogen content limit in extreme environments, suggesting that the polishing process is often not sufficient, and should be adapted to specific operating conditions. However, due to material inhomogeneities such as surface pits and plastic deformation-induced traps, no clear correlation could be established between polished material and bulk hydrogen. Nonetheless, a smooth polished surface was proven to minimize the presence of micro-reaction sites and subsurface defects, thus reducing the absorbed hydrogen. Additionally, corrosive media also affect hydrogen behaviour in the material. In the present work the trapped hydrogen concentration is seen to be dominant, reducing the risk of hydrogen damage. However, reversibly trapped and diffusible hydrogen is also detected, and can be desorbed or redistributed into other trapping sites during the corrosion process.

Acronyms

PP Pulp and paper

CCC Climate corrosion chamber

TDS Thermal Desorption Spectrometry

SAE Society of Automotive Engineers

MET Melt extraction tester

TDS Thermal Desorption Spectrometry

OM Optical Microscopy

SEM Scanning Electron Microscopy

EDS Energy Dispersive X-ray Spectroscopy

XPS X-ray Photoelectron Spectroscopy

TDA Thermal Desorption Analysis

PE Petroleum ether

IPA Isopropanol

Declaration

I hereby declare that except where specific reference is made to the work of others, the contents of this thesis are original and have not been submitted in whole or in part for consideration for any other degree or qualification in this, or any other university. This thesis is my own work and contains nothing which is the outcome of work done in collaboration with others, except as specified in the text and Acknowledgements.

Eider Barazar Garcia

May 2023

Contents

List of Figures

List of Tables

1 Research focus

1.1 Introduction

During the application of bearings, hydrogen is formed from the interaction between the steel and the environment due to electrochemical reactions happening at the surface. The hydrogen is transported by diffusion and localization into the internal sites of the metal and the material becomes more propense to hydrogen enhanced damages [1]. Some issues related to the presence of hydrogen are possible hydride formation, hydrogen mobility, the impact of hydrogen on the stability of the present phases, and the interaction between hydrogen and microstructural defects [2]. Therefore, the characterization of the presence and behavior of hydrogen is of crucial importance.

During corrosion product buildup, certain chemical reactions happen at the surface, which define the characteristics of the formed corrosion product. This happens through a dynamic evolution of the product with exposure time, formed by a combination of various compounds that interact with each other. The formation and rate of hydrogen uptake is not an increasing function of exposure, but is conditioned by the nature of the environment, exposure time, and corrosive agents. Variability of these factors can be related to changes of the mechanism of hydrogen evolution reaction and product buildup [3]. The hydrogen is first adsorbed into the surface, and then can then be absorbed by diffusion through the metallic structure or effused into the environment. The absorption process also depends on the surface material characteristics such as the chemical surface state of the material and the roughness [4].

The recoverability of the mechanical properties can be determined by the amount of hydrogen retained in the material, which must be below a defined limit to avoid quality deterioration of the components. A maximum acceptable amount of 2 ppm of bulk hydrogen is established by the bearing companies to ensure reliable functionality. The amount and distribution of hydrogen in the bulk is defined by the trapping capacity and hydrogen diffusivity in the material. This is influenced by the microstructural characteristics of the steel such as grain size, precipitates etc. [4], and traps generated during service such as traps induced by plastic deformation [5]. The character of the traps conditions the hydrogen distribution and mobility and defines the capacity of migration of hydrogen to the more sensitive zones for hydrogen damage. The hydrogen at reversible traps can be released and can react again during coming applications, while irreversible traps don't interfere in the diffusion process once these are filled [6].

To extend the service life of bearings a remanufacturing process is used to restore

the operating capabilities of the components avoiding a complete replacement of the bearing. The process involves the removal of the corrosion product by polishing until the surface is visually clean, and subsequent finishing of the surface. During the process the removal of a certain amount of base material happens at the interface between the metal and the formed corrosion product. The remanufacturing companies remove the first atomic layers, up to 20 µm, where most of the hydrogen is expected to be placed. However, the hydrogen that remains entrapped in the bulk might still condition bearings operation even if the corrosion product is visually removed. Some of the damage caused by hydrogen in the material may as well be irreversible and lead to further damage from hydrogen uptake in future exposure [7]. Other factors on the material removal process, such as the roughness of the newly generated surface may also influence the hydrogen diffusing out or into the sample [1].

Quantification of the role of hydrogen in steels is still complex due to low contents of hydrogen produced during exposure to corrosive environments, the low sensitivity to external conditions, and to the high mobility of hydrogen atoms in steel [8]. Moreover, hydrogen characterization and measurements show significant scatter due to factors such as the hydrogen charging method, manufacturing process, and material characteristics. The aim of this study is to investigate the behavior of hydrogen in various corrosive environments and to evaluate the effectiveness of the polishing process in avoiding hydrogen enhanced damage and ensuring applicability of remanufactured bearing components. titlesec

1.2 Project background

The absorbed hydrogen is partly determined by the dynamics of the corrosion products formed during exposure. In hardened steel such as AE 52100 steels the corrosion product is expected to be formed by $Fe(OH)^2$, $FeOH^+$,FeOOH, Fe_3O_4 and Fe_2O_3 [9]. During the formation of oxides and hydroxides hydrogen is generated through the cathodic reaction and the hydrolysis, and is adsorbed on the surface by reducing H^+ ions to H_{ads}, Equation 1. The adsorbed hydrogen is then partially desorbed in gas form recombined with another adsorbed hydrogen, H2, or absorbed into the bulk, H_{abs}, as in Equation 2 [10].

$$2H^+ + 2e^- \rightarrow H_{ads} \ , \tag{1}$$

$$2H_{ads} \rightarrow H^2 \tag{2}$$

The amount of absorbed hydrogen is defined by the thickness and stability of the

corrosion product that conditions the diffusivity of hydrogen through the formed compounds [3], and the trapping capacity of the material. This depends on the density of sites available for adsorption and the binding energy of the absorbed hydrogen.

Traps can be categorized by their reversible character based on the probability that a hydrogen atom leaves the site. In reversible traps hydrogen can diffuse in and out due to a low binding energy (<60 kJ/mol). Irreversible traps are those in which the trapped hydrogen is strongly bounded, and the needed activation energy is too high for it to escape (>60 kJ/mol). Hadam et al. [11] addressed that the amount of trapped hydrogen can get to be a majority as high as 85 % of the absorbed hydrogen in carbon steels. Reversible traps usually include micro voids, grain boundaries, dislocations, and coherent precipitates, while irreversible traps can be second phase like carbides, nitrides and oxides [12]. Reversible traps mainly generate elastic distortions, while larger irreversible traps might compromise the mechanical properties of the steel under rolling contact fatigue. However, the danger of reversible hydrogen resides in the capacity of migration to the more sensitive zones [9].

Initially, the diffusivity of hydrogen in the material is expected to be reduced due to the attractive interactions between hydrogen and trap sites. Once irreversible traps are saturated the diffusion rate increases due to the presence of mobile hydrogen, and eventually gets to a steady state. Immediately after exposure the material will contain diffusible hydrogen, which will be effused with time. Later the trapped hydrogen is only detected [5].

The presence of hydrogen is important to consider by itself, but the material's loading history also affects the hydrogen accumulation. Hydrogen trapping is more pronounced in zones that undergo plastic deformation due to the formation of deformation induced trapping sites [13]. There is a higher distribution of volume defects at the surface and subsurface, where hydrogen behaves differently from the matrix. Defects can drastically increase local hydrogen concentrations and play a role as internal hydrogen sources.

The remanufacturing process of bearings through polishing can achieve similar specifications to a new product at 60% off the cost of a new bearing, needing up to 90% less energy [14]. The polishing entails the removal of the corrosion product and a certain amount of base material in the range of 10 - 20 µm [15], addressed by SKF. The removal of the first few atomic layers can entail the reduction of the containing hydrogen as most of it is placed at the subsurface zone. Nonetheless, even if the corrosion product is visually removed from the surface, hydrogen in the bulk might still condition

bearing‘s operation. The remanufacturing process does not ensure the recoverability of the material from previous hydrogen damages that act as hydrogen traps and hydrogen sources in coming applications [7]. Moreover, effects such as plastic deformations and an increase on the surface roughness due to polishing can lead to alteration in the symmetry of the subsurface stress distribution. The redistribution of the stresses can be accompanied with the redistribution of the bulk hydrogen [16].

1.3 Research objectives

The research objectives are stablished to better define the approach and purpose of the study. These will guide the work line followed throughout the research, and will later be used for the evaluation of the accomplishments.

Research gap 1: How do environmental parameters determine the corrosive behavior of the steel? How is the hydrogen content absorbed during the process correlated to the chemical reactions happening at the surface?

- Which are the potential environmental parameters that enhance hydrogen absorption due to corrosion?
- How do environmental parameters change the formed corrosion product?
- How are the composition and morphology of the product related to the amount of absorbed hydrogen? How does hydrogen content evolve with the formation of the compounds?

Research gap 2: Can the remanufacturing process by polishing ensure the needed operating capabilities of corroded bearing for future applications?

- Which are the machining parameters and polishing process followed in the remanufacturing of bearings? How do these affect the amount of hydrogen found in the material?
- How is the reduction of the hydrogen content inside the steel related to the amount of corrosion product and base material removed during remanufacturing?
- Is the hydrogen content inside the remanufactured steel lower than the maximum acceptable hydrogen content defined by the bearing manufacturing companies (2 ppm)?
- Does the polishing process entail any type of surface or subsurface alteration, such as the formation of defects or surface roughness? How are these related to the absorption and content of hydrogen?

Research gap 3: How is the diffusion and accumulation behavior of hydrogen defined by the different conditions to which bearings are exposed?

- Is the absorbed hydrogen found as diffusible or trapped hydrogen?
- What defines this characterization?

1.4 Research outline

The thesis is organized into five chapters that compose the overall of the present research.

- Chapter 1: Research focus: The outlines obtained from the previous literature review are included for their consideration, as well as the research project collaboration and the scope of work. The aim of this chapter is to define the work that will be done in the coming chapters.
- Chapter 2: Materials and methods: The materials used and the mechanism of research are defined. It includes an explanation of the methodology, and the equipment and tools used throughout the study. The atmospheric corrosion of carbon steel is analyzed in detail through exposure of the metal in a climate chamber. The parameters that will define the corrosive environments are specified, such as the type of chemical species and its concentration. Then the formed product and the hydrogen behavior is studied through various equipment.
- Chapter 3: Results: Observation of the results and outputs. The corrosion product morphology, structure, and composition are studied. The remanufacturing through polishing and the effects of the process are analyzed by the evaluation of the response on the hydrogen absorption.
- Chapter 4: Discussion: The results in the previous chapter are considered as a guidance for the estimation and evaluation of the effect of corrosion phenomenon.
- Chapter 5: Conclusions and Recommendations: The overall outcomes of the research work are discussed and summarized. Recommendations and considerations for future research are included.

2 Materials and Methods

2.1 Research material

All the bearings used throughout the present work are bearings provided by SKF, obtained from their industrial bearing remanufacturing centre in Steyr, Austria. The material used is from two primary bearings, namely bearing A and bearing B, which exhibit distinct levels of corrosion. Both are spherical roller bearings (SRB) with two rows of symmetrical rollers as the one shown in Figure 1.

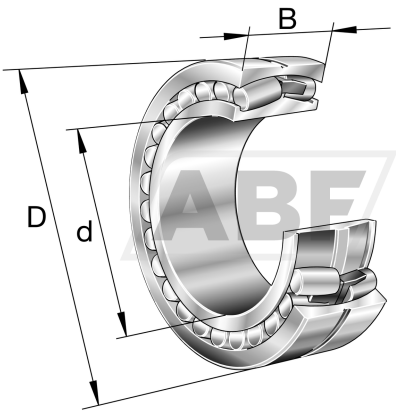

Figure 1: *FAG 239/560-B-K-MB-C3 ring [17].*

In both cases the investigation is focused on the inner ring of the bearings. Bearing A, Figure 2, displays minimal corrosion marks while bearing B, Figure 3a, is markedly affected by corrosion. Figure 3b show a closer look of the corrosion patterns observed on bearing B.

Figure 2: *Slightly corroded bearing from Steyr, bearing A.*

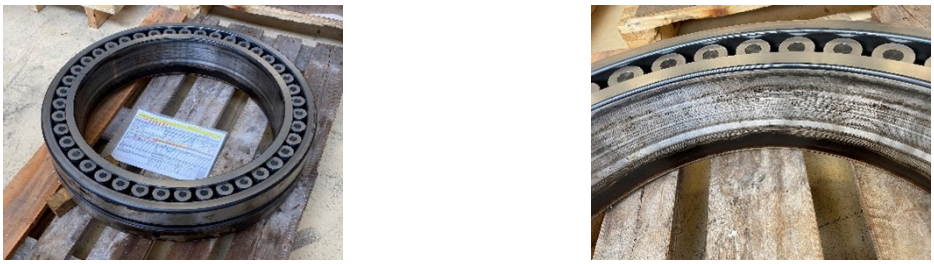

(a) (b)

Figure 3: (a) *Corroded bearing from Steyr, bearing B.* (b) *Closer look of Corroded bearing from Steyr.*

Some data about the material and the environmental conditions to which bearings are exposed is not detailed or complete. This leads to some information being unknown throughout the study. Both bearings have been corroded while applied in Pulp and paper (PP) industry, not necessarily under equal conditions. The specific model of bearing A is unknown. It has an outer diameter (D) of 595 mm, an inner diameter (d) of 540 mm, and a width (B) of 135 mm. The bearing B belong to a competitor company, FAG, model 239/560-B-K-MB-C3, with an outer diameter (D) of 750 mm, an inner diameter (d) of 560 mm, and width (B) 140 mm [linkbearing]. The material from bearing A is a Grade 5 steel based on the Society of Automotive Engineers (SAE) classification system, with an element concentration in % shown in Table 1. The material of bearing B is a Grade 4 steel, Table 2. The chemical composition was addressed through a Spectrometer by pointing at 7 locations in Bearing A and 5 locations in Bearing B. The main chemical difference between both bearings is the carbon content; 0.9610 % in Bearing A and 2.916 % in Bearing B.

Table 1: *Chemical composition in % of Bearing A, Grade 5 steel.*

Fe	**C**	**Si**	**Mn**	**Cr**	**Ni**	**Mo**
-	0.960	0.27	0.49	1.60	0.17	0.15
P	**S**	**Co**	**V**	**W**	**B**	**N**
0.012	0.010	0.015	0.010	0.01	0.0001	0.0663

Table 2: *Chemical composition in % of Bearing B, Grade 4 steel.*

Fe	**C**	**Si**	**Mn**	**Cr**	**Ni**	**Mo**
-	2.916	0.45	0.76	1.40	0.11	0.03
P	**S**	**Co**	**V**	**W**	**B**	**N**
0.011	0.008	0.011	0.005	0.01	0.0001	0.0969

2.2 Methodology

Table 3 lists the tests and analyses performed where: X ; test conducted, and - ; test not conducted. The equipment used throughout the work includes the Climate corrosion chamber (CCC), Optical Microscopy (OM), Scanning Electron Microscopy (SEM), Energy Dispersive X-ray Spectroscopy (EDS), Melt extraction tester (MET), and Thermal Desorption Spectrometry (TDS).

Table 3: *Overview of the tests and analyses performed throughout the investigation.*

	Corrosion conditions	**Corrosion indicators**	**CC**	**OM**	**SEM**	**MET**	**TDS**
Reference Bearing A	No/very little corrosion from application	No visible corrosion	-	X	-	X	X
Corroded Bearing B	Corrosion from application	Visible corrosion	-	X	-	X	X
Artificially corroded Bearing A	Corrosion from s extreme condition	Visible corrosion	X	X	X	X	X

To study the formation of the corrosion product in different environments samples are placed in a WT3 180/40 climate chamber from Weiss Techniq. The WT3 180/40 is a environmental testing chamber used to simulate specific temperature and humidity conditions, at temperatures (T) between - 40 °C and 180 °C, and humidity levels between 20% and 98% relative humidity (RH) [18]. The chamber is used to test the durability and reliability of the material under extreme environmental conditions.

When in service in the P&P industry, environmental parameters can change according to the position of the bearing. Temperature can be in the range from 40 °C to more than 180 °C, with a varying humidity (around 100% on paper machines). The environmental pH depends on the type of paper, which usually ranges from 3 to 8. Moreover, processed water may contain very different chemical elements [15].

The process followed in this work is detailed in Figure 4. Before the exposure of the samples these are cleaned on Petroleum ether (PE) and Isopropanol (IPA) on an ultrasonic bath. Then all surfaces are sprayed with a protective surface coating, **??**, limiting the exposure to the top surface. The applied coating is the CROP 1K Anti Corrosion Primer, a rust-inhibiting primer designed to protect metal surfaces from corrosion. The primer creates a barrier between the metal and the environment preventing moisture and other corrosive agents from coming into contact with the substrate. This

is a one component primer that is applied directly to the surface of metal and dries in approximately 2 hours.

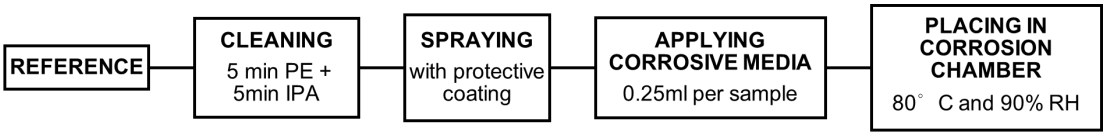

Figure 4: *Overview of the process followed before placing the samples in the atmospheric corrosion chamber.*

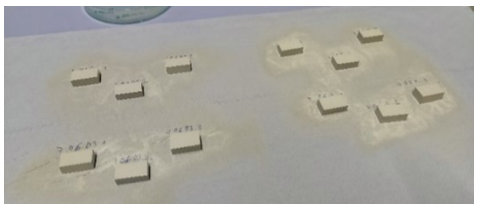

Figure 5: *Samples sprayed with CROP 1K Anti Corrosion Primer.*

Four different environments were simulated in the corrosion chamber by applying 4 different corrosive medias: pH 1.5 in H_2SO_4, 3.5 in H_2SO_4, and pH 7 0.1 M NaCl and 0.6 M NaCl. The corrosive media was deposited on the exposed surface through a syringe, applying 0.25 ml per sample once before these are placed in the chamber for a defined period of time. The specimens were exposed in the corrosion chamber under 80 °C and 90% RH. These values were agreed based on the information provided by Steyr about the application and conditions in PP, previously commented in this subsection. The temperature and RH were maintained constant, with only major variations as a result of the removal of other samples from the chamber. These variations are not considered in the study. The samples were kept in the chamber for a specific period of time between 3 and 18 days. The samples immersed in different solutions and exposure times are classified in Figure 54.

2.2.1 Optical microscopy (OM)

Every sample, corroded and non-corroded, is analyzed by the optical microscopy (OP) for a further characterization of the formed corrosion product. The used microscope is the LEICA (Leica Microsystems Digital Microscope), a type of digital microscope that combines a traditional microscope with digital imaging technology. Images of the specimens are captured with the digital camera to analyze the amount and distribution of the corrosion product.

2.2.2 Scanning electron microscopy (SEM)

Not all features can be characterized by the OM and the Scanning electron microscope (SEM) is used for further characterization. The Thermo Fisher Teneo Scanning Electron Microscopy (SEM) is used to produce high-resolution images. This method allows the magnification of the sample to a nanometer-scale through the interaction of an electron beam with the surface atoms at different depths. SEM provides a further characterization of the rust layer through a physical observation and evaluation of crystalline phases based on research literature from previous investigations. These are later related to the formation dynamics of the corrosion product and the hydrogen generation during the chemical reaction process.

2.2.3 Energy Dispersive X-ray Spectroscopy (EDS)

The SEM technology also offers advanced imaging capabilities such as Energy Dispersive X-ray Spectroscopy (EDS) for chemical analysis. This is an analytical technique used to identify and quantify the elemental composition of the corrosion product. The X-rays emitted by irradiating the sample with a beam of electrons are unique to each element, and it is possible to identify the elements present by measuring their energy. The technique is used in conjunction with SEM for accurate mapping of the elemental distribution within a sample. It needs to be considered that very light elements are often not detectable as these don't have electrons in an outer shell, and consequently characteristic X-rays cannot be emitted.

2.2.4 X-ray Photoelectron Spectroscopy (XPS)

The X-ray Photoelectron Spectroscopy (XPS) technique is used to characterize the corrosion product by the identification of the chemical compounds. X-rays interact with the sample and detect the kinetic energies of electrons to measure the chemical state of atoms. The PHI VersaProbe Scanning XPS System is used, operated with PHI Summitt and Vacuum Watcher software programs. The data reduction and interpretation are carried out using MultiPak, a MatLab-based program that employs a peak identification algorithm within its data reduction package.

First a controlled erosion of the surface is performed through ion sputtering, which removes surface contamination and loosely bound species. A monochromate Al-Kα ($\approx$ 1486.7 eV) X-ray excitation source is applied, operated at different voltages in each analysis. The quantification process is done by combining the obtained spectra with recorded experimental data from literature, Moulder et al. [19]. The adventitious carbon signal is used as reference for charge shift correction, and surface charging effects

are compensated by referencing the binding energy (BE) to the C 1s line of carbon set at 284.8 eV.

The samples are analyzed one day after being removed from the chamber, time required for the equipment to pump down and get to the necessary vacuum level. The sample is placed on the specimen holder with stickers attached to the base. As the surface composition is initially unknown, a broad scan survey spectrum is performed to identify the elements. Then a detailed scan of the selected peak locations is carried out. The spectrum plots the number of electrons vs. the electron binding energy. Two main scans are carried out for each of the three zones, one before and one after sputtering. The photons have limited penetrating power in a solid on the order of 1 - 10 micrometers. During sputtering, a controlled erosion of the surface is done, which helps to better define the depth profile.

2.2.5 Melt extraction tester (MET)

The hydrogen concentration in the material is analyzed in the Eltra ONH-2000 melt extraction tester by heating and melting the sample in an electrically heated graphite crucible. Before the carrier gas enters the furnace, the graphite crucible is heated up in the furnace to remove impurities, and the base lines of the detectors are stabilized. The sample (1g) is dropped into the crucible by a rotation mechanism. The process involves the heating of the sample by the fusion of inert gas in an impulse furnace, with current electrodes that heat the graphite crucible by resistance up to 3000 °C [1]. The sample is melted and the released gases like hydrogen, oxygen and nitrogen are measured by the thermal conductive detector.

Calibration of the equipment is performed by certified reference materials. Materials from ELTRA with certified hydrogen concentrations are analyzed. For an empty crucible H $<$ 0.3 ppm and O $<$ 2 ppm values are taken for a manually introduced input weight of 1 g. The standard material used contains H = 7.4 $\pm$ 0.6 and H = 2.5 $\pm$ 0.3 ppm, and O = 30 $\pm$ 2 ppm (specified in each test). Several empty and reference sample tests are performed in an interspersed manner until measured values agree with the certified values. The hydrogen in the reference samples is chemically bonded, and therefore is not able to be released at room temperature even after a very long time [thesisblanca]. Before the measurements all samples are cleaned in the ultrasonic cleaner. These are first immersed in PE for 5 minutes, dried, immersed in Acetone for 5 more minutes, and dried again.

The cleaning of the hydrogen analyzer is important for the measurement accuracy.

The reagent tubes are glass tubes filled with chemicals that periodically need to be replaced. First the dust trap needs to be checked and filled with glass wool. Moreover, another reagent tube is replaced with Schutzes reagent, with glass wool at the tube ends. The furnace is recommended to be cleaned at least every 50 analyses, but this should be cleaned more often if there is a high content of dust.

2.2.6 Thermal desorption analysis (TDA)

The Thermal Desorption Analysis (TDA) studies the escape reaction of hydrogen from a trap by heating of a material. In metals, hydrogen transport is strongly affected by the type of hydrogen trapping sites, characteristic of each microstructure. The TDS gives information about the distribution of internal hydrogen by giving sufficient supply for the ejection from interstitial and trapping sites where hydrogen resides. The hydrogen is "deactivated" at different temperatures depending on the trapping energy.

The system used in the CDS Analytical Pyroprobe 5000, Figure 6, a multiple step, platinum filament pyrolysis instrument performs sample analysis by gas chromatography. The equipment is conformed by the pyroprobe unit (PU) and the gas chromatography unit (GC). The temperature of the filament is regulated by the microprocessor of the Pyroprobe 5000, by calculating the resistance of the filament at set point temperature and supplying the correct voltage to achieve the desired temperature of the filament. In the present work a coil probe is used for pyrolysis of samples in a quartz tube. The Pyroprobe 5000 is connected to a Agilent 7890A gas chromatograph via a heated chamber that encloses the filament rod during the pyrolysis process. The Pyroprobe 5000 is interfaced to a Agilent 7890 A chromatograph, controlled by an attached data system, ChemStation. The temperature of this interface, as well as the temperature of the pyrolysis filament is predetermined based on the applied method and remains constant throughout the analysis. Each method includes an initial temperature, a heating ramp, and a final temperature for the Pyroprobe filament.

Before a measurement the equipment is calibrated to get reference for the hydrogen peaks and define the amount of hydrogen in the sample. To determine the relation between the raw signal from the thermal conductivity detector and the hydrogen released from the sample, the equipment has a gas calibration module used to inject defined amount of calibration gas of known hydrogen content into the carrier gas [1]. The obtained sum of areas of hydrogen peaks from the calibration will be used in the hydrogen content calculation later described in 2.3.1 Thermal desorption analysis (TDA). The calibration runs for 90 min, during which the hydrogen content is measured within 3-

Figure 6: *CDS Analytical Pyroprobe 5000 system. Equipment used for the Thermal Desorption Analysis (TDA).*

minute intervals. In each interval three peaks are detected corresponding to hydrogen, oxygen, and nitrogen gases, illustrated in Figure 7. The measurement is performed 3 times in 3 different samples in order to study the replicability.

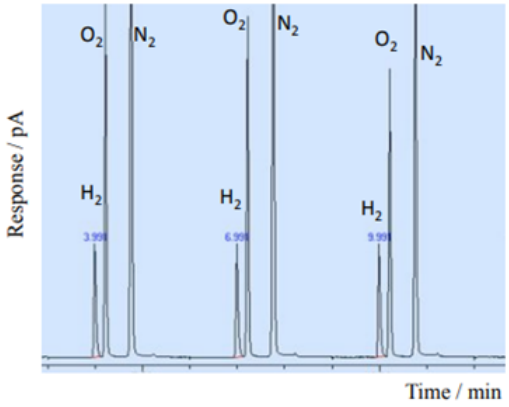

Figure 7: *Peaks obtained from calibration of the equipment. A measurement is performed within 3 minute intervals, where three peaks are detected corresponding to hydrogen, oxygen and nitrogen gases [20].*

The hydrogen analysis is done at 2 different timings; immediately after taking samples out of the chamber and 24 h after. The aim is to understand the behavior of the hydrogen inside the sample before allowing enough time for it to diffuse out at room temperature. The results are then compared to the hydrogen found after 24 h of charging and surface polishing. The time between charging the TDA test can be called degassing time. The degassing time between samples being taken out from the chamber and the TDS test is estimated to be 20 minutes, 120 minutes and 200 minutes for the first timing, considering the sample preparation and testing time.

In the present study the test is run for 90 minutes as follows: initial temperature 27 °C, heating ramp 5°C/min, final temperature 400 °C. These specific parameters were defined by SKF, based on previous performed tests and literature. For the data interpretation the obtained spectra are visually analyzed. The peak fitting and calculation

of the corresponding activation energies is beyond the scope of the present work. The aim is to observe if the environmental characteristics have an effect on the trapping of hydrogen, and how might this be influenced. The peaks are analyzed considering temperature ranges, and concluding on the trapping behavior by comparison of results obtained at different corrosive environments.

Before every measurement samples are cleaned with petroleum ether (PE) and acetone to remove any layer of impurity which may have been deposited on the surface. The aim is to first check the hydrogen behavior inside the sample before allowing sufficient time for the hydrogen to diffuse out at room temperature. These results are then compared to the ones obtained after 24 h, where most of the hydrogen is already diffused, and the hydrogen that stays correspond to trapped hydrogen with higher binding energies.

2.2.7 Sample preparation

Both inner rings from bearings A and B are cut into 30 mm thick segments. Figure 8a shows a segment obtained from Bearing A, and Figure 8b a segment from Bearing B, severely corroded.

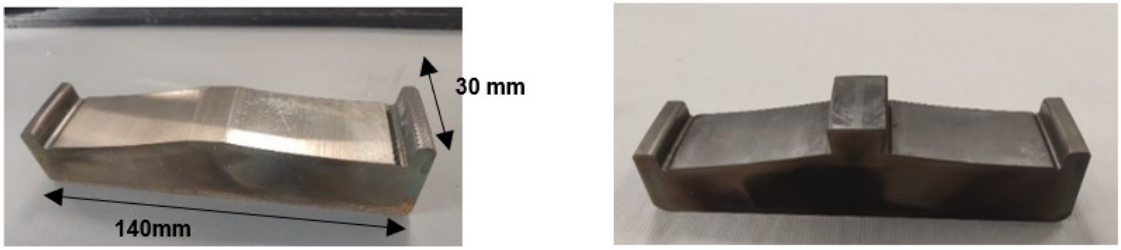

(a) (b)

Figure 8: (a)*Segment from Bearing A, non-corroded* (b) *Segment from Bearing B, corroded in P&P industry*

The segments are then cut again into smaller samples, Figure 9, of size 30 x 15 x 10 mm with an abrasive cutting machine. The samples and corresponding measurements are illustrated in Figure 10. These samples will be exposed in the climate chamber in sets of three.

Due to the size limitations of the MET, TDS and XPS techniques, specimens need to be cut again. In the MET and TDS the required samples dimensions are 10 x 4 x 3.5 mm. These measures are defined in order to fit the samples in the graphite crucible used in the MET and the quartz tub used in the pyrolysis unit in the TDS. 3 sub-samples are obtained from previously cut samples, illustrated in Figure 11. The samples are cut in a way that the corroded top surface of 10 x 4 mm^2 is maintained unaffected for its

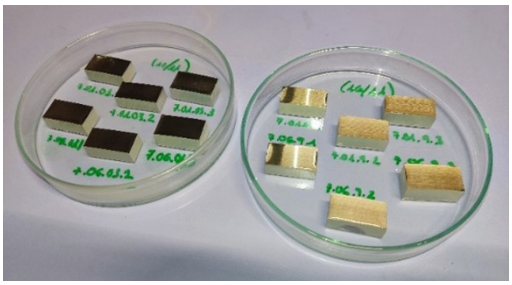

Figure 9: *Samples to be placed in the chamber.*

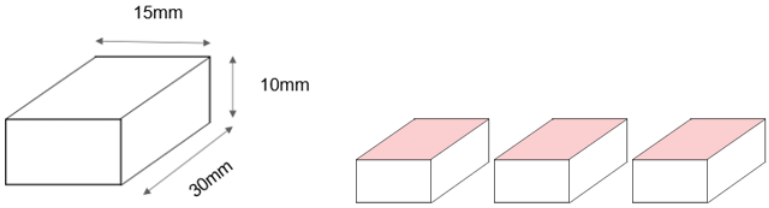

Figure 10: *Measurements of the samples to be exposed in the climate chamber. These are placed in sets of 3. The top red surface represents the exposed surface.*

analysis. For the XPS the specimens need to be placed in a slot of 20 x 10 x 6 mm, Figure 12.

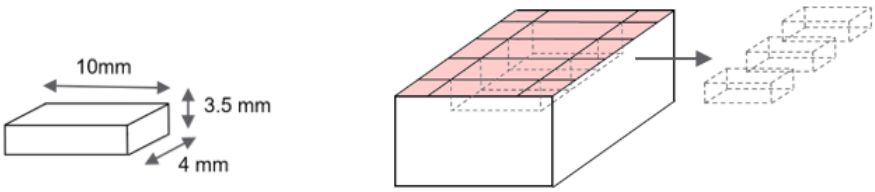

Figure 11: *Subsamples for the MET and TDS, obtained from samples previously cut. The top red surface represents the exposed surface.*

2.2.8 Polishing

The removal of the corrosion product is done by mechanical polishing with fine grain silica carbide (SiC). The polishing is performed at two different timings based on the purpose of the process. In METHOD 1 the effect of polishing of the product is intended to be understood. For this, as a simulation of the remanufacturing process, samples are polished only after these are exposed to the corrosive environment. A single polishing process is followed throughout the procedure. In METHOD 2 the effect of the surface roughness before exposure is analyzed. For this, samples are polished before being placed in the chamber, and after their exposure for the hydrogen measurement. Two polishing processes are performed this last time. The comparison between METHOD

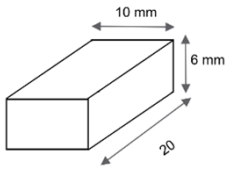

Figure 12: *Samples for the XPS.*

1, Figure 13a, and METHOD 2, Figure 13b, is used to understand if the exposure of the newly generated surface surface has an effect in the hydrogen absorption.

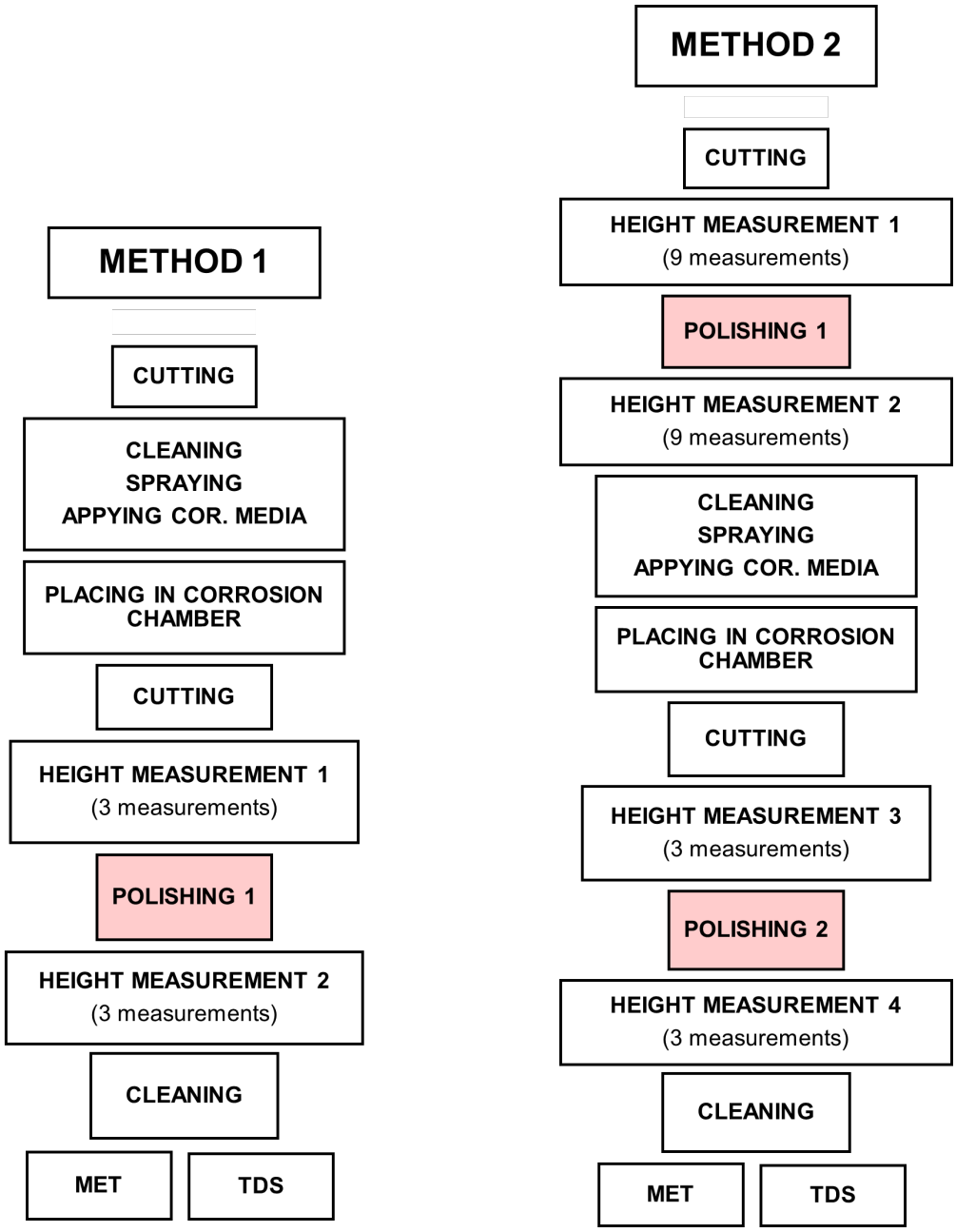

(a) (b)

Figure 13: (a)*Step by step illustration of METHDD 1, polished after corrosion exposure.* (b) *Step by step illustration of METHDD 1, polished before and after corrosion exposure.*

In all polishing processes the surface is polished until the corroded surface is visually clean, free of any corrosion product. The removed product is studied by measuring the height of the samples before and after polishing. The height average value is obtained by measuring different points in a sample (corners and middle) out of three different samples. For the study of the effect of polishing after exposure (METHOD 1), the samples are cut into small subsamples. The heigh change is measured before and after

polishing in 3 different locations. The effect of roughness (METHOD 2) is studied in samples polished before being placed in the chamber. 9 points of the surface are measured in order to cover the whole surface. Both polishing methods are illustrated in Figure 14. Before every heigh measurement the samples were cleaned ultrasonically for 2 minutes in a bath of PE.

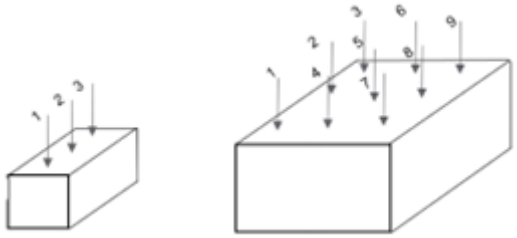

Figure 14: *Illustration of locations for heigh measurements in METHOD 1 (left) and METHOD 2 (right).*

2.3 Calculations

2.3.1 Thermal desorption analysis (TDA)

A steel material has several kinds of traps and lattice sites where hydrogen can be placed. These traps can be classified according to their activation energy for hydrogen trapping. The spectrum usually presents not only one but several desorption peaks corresponding to each site, which need to be individually characterized. The hydrogen released from the trap usually has a Gaussian distribution, which is a symmetric peak. The spectrums are interpolated by a sum of a given number of Gaussian peaks, each representing an absorption site in the material.

The results obtained from the TDA are plotted as the response of each gas in pA (picoampere) in the Y axis and the retention time in min the X axis. The valve box allows a 0.5 ml gas sample from the loop to be injected into the column to be analyzed by the detector for 3 minutes. The procedure is repeated throughout the whole process. Again, in every measurement, hydrogen, oxygen and nitrogen gases are evaporated and carried by the helium carrier gas to the column. This is represented by numerous sets of three peaks that are repeated every 3 minutes.

The areas of the hydrogen peaks from the calibration are used for the calculations. The integrated area of the peak of a standard, which is constant during the analysis, is compared with the integrated area for each peak from the investigated sample analysis. From the calculations the amount of hydrogen desorbed from the sample and its vari-

ation with temperature can be known, from which the trap nature can be determined.

The calibration gas used is H_2/He, is 10.2 µmol of hydrogen in 1 mol of helium. This concentration correspond to each integrated peak of the standard. The average area of the integrated peaks of the calibration (AC) is 10.2×10^{-6} mol. Using the values in Table 4 the calculations proceed as follows [20]:

Table 4: *Hydrogen content determination in TDS.*

	Helium	Hydrogen	Area
Steel sample	12 ml/min (8.928×10^{-6} mol/s)	X (mol/s)	Peak of analyzed steel sample (SA) (pA*min)
Calibration gas	1 mol	10.2×10^{-6} mol	Average of calibration (AC) (pA*min)

Considering 1 mol of any gas occupies 22.4 L of volume, and that 12 ml/mol = 0.2 ml/s the helium on the steel sample can also be written as;

$$He_s = \frac{0.2\,ml}{s}.\frac{1\,mol}{22400\,ml} = 8.928x10^{-6}\,mol/s \tag{3}$$

Considering the hydrogen concentration is proportional to the area the hydrogen content in the steel sample (X) is calculated as follows;

$$\frac{X}{8.928x10^{-6}\,mol/s} : \frac{10.2x10^{-6}\,mol}{1\,mol} = SA\colon CA \tag{4}$$

$$X = \frac{10.2x10^{-6}\,mol * SA}{8.928x10^{-6}\,mol/s * CA} \tag{5}$$

As 1 mol of H_2 equals 2g and considering the sample weight;

$$X(ppm/s) = \frac{10.2x10^{-6}\,mol * SA}{8.928x10^{-6}\,mol/s * CA} * \frac{2g}{(sample\,weight)g}x10^{-6} \tag{6}$$

By multiplying the result by 3 minutes the amount in ppm is obtained for the considered peak. The calculations need to be repeated for every peak collected from the sample, and sum them up to obtain the total hydrogen content.

In the present work the hydrogen is released continuously from the sample with a time and temperature increase of 5 °C/min. The sample is heated up from 30 °C to 400 °C, and maintained at this temperature for 10 minutes. Relating the process to the retention time the peak temperatures at which the hydrogen scape are calculated and plotted.

$$T(^oC) = 30\,(^oC)\ +\ retention\,time\,(min)\,x\,5\,(^oC/min) \tag{7}$$

3 Results

The research investigation is divided into three parts based on the levels of corrosion in the bearings. Initially, an analysis of the non-corroded reference Bearing A is done, followed by the analysis of the corroded Bearing B used in pulp and paper application, and lastly, the reference Bearing A exposed to corrosion under controlled conditions.

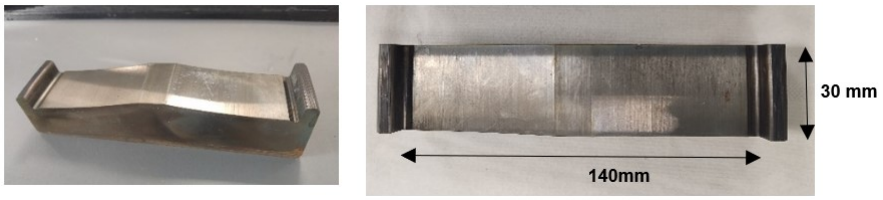

Figure 15: *Lateral and top view of segments obtained from the non-corroded/reference bearing, Bearing A.*

To analyse the corrosion in application, a corroded bearing employed in the pulp and paper (P&P) industry was received from Steyr, Bearing B, shown in Figure 16. The bearing could have been subjected to environments containing diverse chemical elements during its application. However, the company providing the bearing did not specify any information regarding the nature of the environments. The temperature range to which the bearing was exposed can vary from 40 °C to over 180 °C, with a humidity fluctuating around 100 %. The environmental pH typically ranges from 3 to 8.

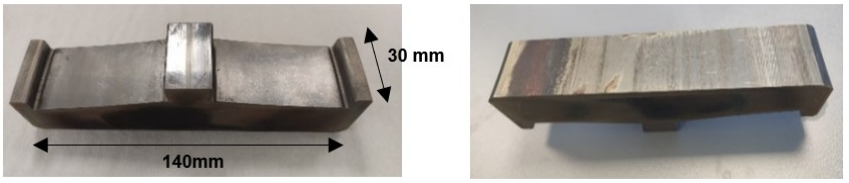

Figure 16: *Lateral and top view of a segment obtained from the corroded bearing, Bearing B.*

Corrosion is visibly present in both the front raceway and the back surface in contact with the shaft, with the latter exhibiting more pronounced signs of corrosion. Given the apparent differences in the extent of corrosion, the bearing segments were divided into distinct sections to facilitate their examination. The raceway was subdivided into three discrete zones based on location. denoted as left (CL), middle (CM), and right (CR), while the back surface was divided into three zones based on the observed degree of corrosion. These zones were designated as CBK1, CBK2, and CBK3, with CBK1 being the most corroded region. The specific sections of the bearing for analysis are illustrated in Figure 17.

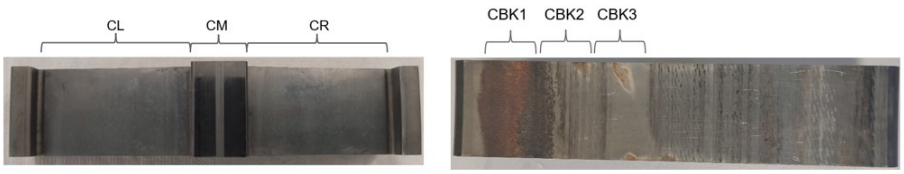

Figure 17: *Illustration of considered zones for study in raceway (left) and back (right) sides of the bearing segment (140 mm x 30 mm).*

To assess the impact of extreme environmental conditions samples from the non-corroded reference bearing, Figure 15, were exposed to a controlled environment within a climate chamber. The study comprised four experimental conditions, all of which were characterized by a constant temperature (T) of 80 °C and a relative humidity (RH) of 90 %. The corrosive solutions employed in the study are pH 1.5 H_2SO_4, pH 3.5 H_2SO_4, pH 7 0.1 M NaCl, and pH 7 0.6 M NaCl.

3.1 Quantification of absorbed hydrogen in the bearing steel

The separate hydrogen and oxygen contents in the material were assessed through the Melt Extraction equipment (MET). The calculation of the content in the samples considering the weight is automatically done by the software. For every considered hydrogen and oxygen content three measurements are done, from which an average value is obtained. This average value is the one considered in the results. Then, samples are subjected to polishing to replicate the remanufacturing process with the aim of correlating the amount of material removed with the hydrogen content left in the metal.

3.1.1 Quantification of absorbed hydrogen in the as received non-corroded bearing

Table 5 presents the hydrogen and oxygen contents in Bearing A, from 10 tests under equal conditions. All samples are obtained from a similar zone of the non-corroded bearing. Each test consists of 3 measurements, resulting in a total of 30 recorded measurements. The considered results are average values of these 3 measurements. The table includes the test number (1 to 10), the average hydrogen and oxygen contents for each test (ppm) and the corresponding standard deviation (SD). The oxygen in ppm is used to evaluate if there is any corrosion product present at the surface. High oxygen contents corresponding to oxides that combine to form the product can show high hydrogen contents due to hydrogen accumulation in the product, not in the bulk. This last is the hydrogen considered in the present study.

Both hydrogen and oxygen, and corresponding deviations are illustrated with respect

to the test number in Figure 18 and Figure 19 respectively. Considerable fluctuations are observed in some of the measurements. The maximum average hydrogen happens in test 6 (1.94 ppm), whereas the lowest is observed in test 10 (0.77 ppm), with a difference of 1.17 ppm between maximum and minimum. This value of 1.17 ppm is significant considering the low hydrogen contents considered in the present work (up to 2 ppm), and high scatter between tests. Furthermore, in tests 2, 5, and 6, even if the average results considered don't overpass the 2 ppm, individual hydrogen values exceeded the acceptable limit. Oxygen stays between a maximum of 20.57 (test 4) and 6.01 (test 9). The highest oxygen content does not agree with the highest hydrogen content (test 4 vs test 5). Nonetheless, the lowest oxygen agrees with one of the samples with less hydrogen found (test 9).

Table 5: *Hydrogen (ppm), oxygen (ppm) and SD in non-polished reference Bearing A.*

	Reference	
Test	Hydrogen (ppm)	Oxygen (ppm)
1	1.2 ± 0.8	6.5 ± 2.6
2	1.6 ± 0.6	11.2 ± 7.5
3	1.4 ± 0.5	10.7 ±1.7
4	1.4 ± 0.2	20.6 ± 8.2
5	1.5 ± 1.2	11.3 ± 0.4
6	2.0 ± 0.6	12.5 ± 3.8
7	1.2 ± 0.2	13.3 ± 1.2
8	1.5 ± 0.5	8.4 ± 0.2
9	0.8 ± 0.0	6.0 ± 1.9
10	0.8 ± 0.1	6.8 ± 4.4

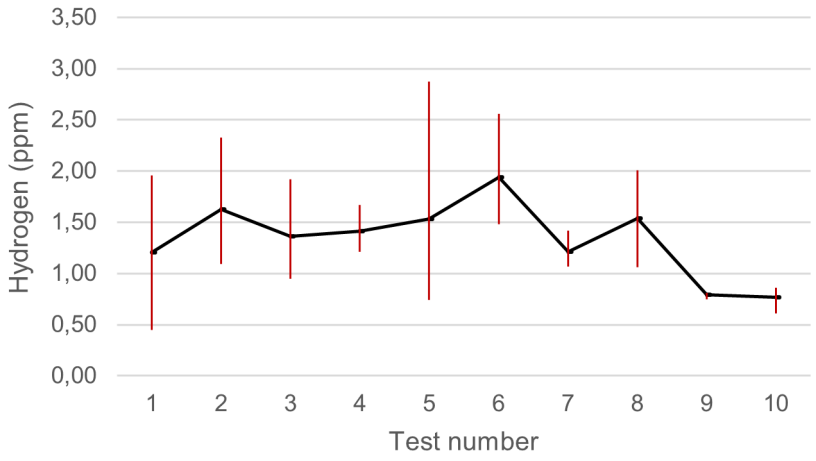

Figure 18: *Hydrogen (ppm) and SD in non-polished reference Bearing A for each test number (1 to 10).*

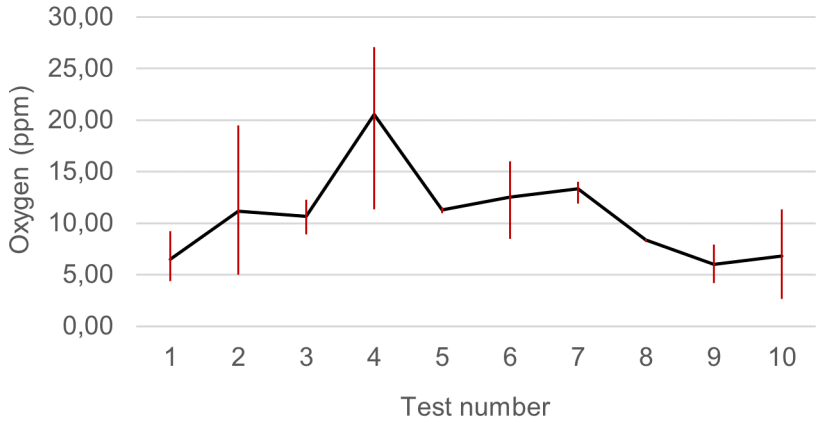

Figure 19: *Oxygen (ppm) vs. test number and deviation in non-polished reference Bearing A for each test number (1 to 10).*

In the remanufacturing simulation of the reference material (Bearing A) the amount of material removed during polishing was restricted to a maximum of 100 µm, as the remanufacturing company removes up to 20 µm of base material in practice. A wider range was considered for a more comprehensive analysis. The results are presented in Table 6, where the amount of removed material is divided into 10 µm ranges. Into parenthesis, the number of tests performed for each range.

Table 6: *Hydrogen (ppm), oxygen (ppm), polished material (µm) and SD in polished reference Bearing A. The number in () indicates the number of tests performed.*

Range (µm)	Tests	Polished material (µm)	Hydrogen (ppm)	Oxygen (ppm)
0 – 10	(2)	8 ± 1.6	0.6 ± 0.2	5.5 ± 1.3
10 – 20	(1)	18 ± 0	0.9 ± 0.0	6.1 ± 0.0
20 – 30	(3)	27 ± 1.9	0.8 ± 0.3	3.3 ± 3.1
30 – 40	(3)	36 ± 0.9	1.3 ± 1.0	7.8 ± 4.8
40 – 50	(1)	48 ± 0.0	1.0 ± 0.0	6.4 ± 0.0
50 – 60	(3)	56 ± 1.2	1.0 ± 0.1	4.9 ± 0.8
60 -70	(3)	65 ± 4.2	0.7 ± 0.3	4.7 ± 1.6
70 - 80	(3)	75 ± 1.8	0.9 ± 0.1	4.0 ± 1.0
80 - 90	(2)	84 ± 0.5	0.8 ± 0.3	4.8 ± 4.6
90 - 100	(3)	95 ± 4.8	0.9 ± 0.4	7.9 ± 7.6
> 100	(3)	103 ± 5.2	0.6 ± 0.0	3.2 ± 0.3

The hydrogen and oxygen (ppm) vs the polished material (µm) are plotted in Figure 20 and Figure 21. A big scatter of data points was observed, and in some cases, such as in the range of 30-40 µm, hydrogen overcame the 2ppm limit. High values of hydrogen agree with high values of oxygen, indicating that the corrosion product was

not completely removed and there is some still left on the surface. After the removal of some more material (40 µm on), a linear trend was visible. Hydrogen content decreases as the removed material increases. Nonetheless, the considered contents are too small and the scatter too notable to make any solid statement. No significant conclusions can be drawn and more tests need to be performed.

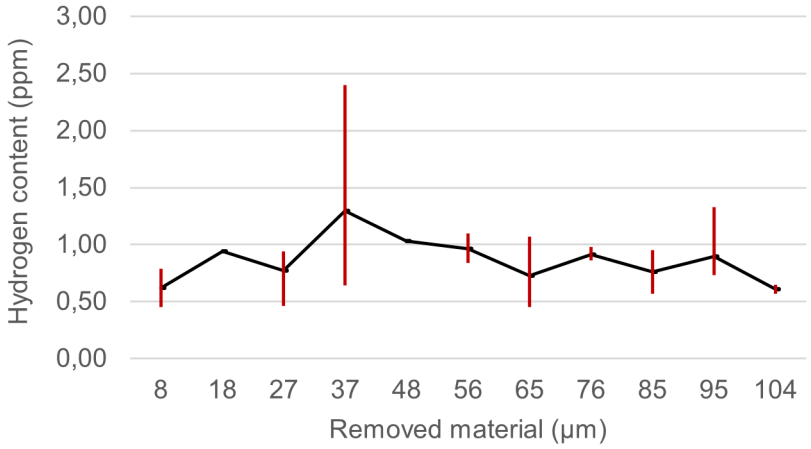

Figure 20: *Hydrogen (ppm) vs. polished material (µm) and corresponding deviation in polished reference Bearing A.*

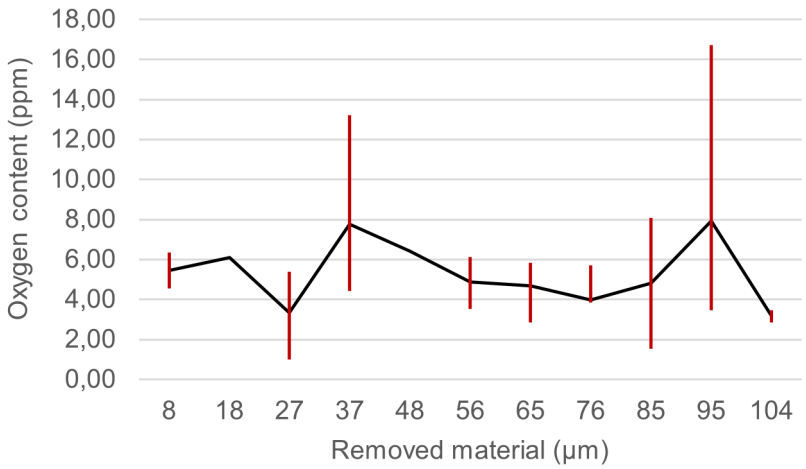

Figure 21: *Oxygen (ppm) vs. polished material (µm) and corresponding deviation in polished reference Bearing A.*

3.1.2 Quantification of absorbed hydrogen in the bearing corroded in pulp and paper (P&P) industry

Table 7 presents the hydrogen and oxygen (ppm) levels detected in the corroded bearing provided by Steyr. Each result and SD correspond to three measurements of from each

considered area. The hydrogen and oxygen concentrations in CL (left), CR (right) and CM (middle) are found to be similar. Notably, the regions of the bearing that were in contact with the shaft display higher levels of hydrogen due to the presence of more corrosion product at the surface. CBK1 exhibits the highest hydrogen, which progressively decreases to CBK2 and CBK3, being consistent with the visual inspection. Moreover, the raceway of the corroded bearing exhibits comparable oxygen concentrations as in the non-corroded bearing, indicating that oxides are still not significantly developed. Very elevated oxygen values are once again detected in CBK1 and CBK2 due to oxides forming the product.

Table 7: *Hydrogen (ppm), oxygen (ppm) and SD in non-polished corroded Bearing B.*

	Hydrogen (ppm)	Oxygen (ppm)
CL	2.0 + 0.2	12.5 + 4.3
CM	1.1 + 0.1	8.6 + 0.6
CR	1.2 + 0.2	11.6 + 1.0
CBK1	74.3 + 5.7	1746.9 + 99.5
CBK2	5.7 + 1.1	264.5 + 43.8
CBK3	1.2 + 0.1	9.5 + 1.3

Subsequently, the samples were equally divided into zones (CL, CM, CR, CBK1, CBK2 and CBK3) and manually polished to analyze the hydrogen stored in the bulk. The hydrogen and oxygen concentration (ppm) and the corresponding polished material (µm) are presented in Table 8. The polishing process is followed until the corroded surface is clean. This can be different in each zone as the need of remanufacturing might be different. Only a visual inspection was used to asses that there was not any corrosion product left in the surface. No other technical equipment.

Table 8: *Hydrogen (ppm), oxygen (ppm), polished material (µm) and SD in polished corroded Bearing B.*

	Hydrogen (ppm)	Oxygen (ppm)	Polished material (µm)
CL	0.9 ± 0.1	2.7 ± 2.1	51 ± 34.5
CM	0.9 ± 0.1	3.83 ± 1.8	53 ± 37.3
CR	0.9 ± 0.0	3.60 ± 0.8	67 ± 19.3
CBK1	1.2 ± 0.8	16.20 ± 10.5	96 ± 30.0
CBK2	1.1 ± 0.2	2.53 ± 1.2	47 ± 53.0
CBK3	1.7 ± 0.3	1.34 ± 0.7	42 ± 49.8

More material needed to be removed from the raceway (CL and CM) than in CBK2 and CBK3, despite these latter exhibiting a greater presence of corrosion product. This difference can be attributed to a greater density of pits in CL and CM, needing additional polishing. Other than that, it is noteworthy that the maximum amount of

material was removed from CBK1, with nearly double quantities. Most of it corresponds to the corrosion product.

From the present testing can be concluded that the remanufacturing of the corroded bearing through polishing looks to be sufficient to ensure that hydrogen stays under the 2 ppm. Hydrogen would noticeably overcome the limit in the non-polished corroded material (Table 7), but this was completely removed with polishing (Table 8). It also needs to be considered that the present bearing was not badly damaged from corrosion. Hydrogen in the raceway was seen to be under the established limits even before the remanufacturing process. This might not be the case in bearings exposed to more extreme conditions, where the tested remanufacturing process might not be enough. No details were provided about the application in pulp and paper industry, and therefore the hydrogen and corrosion product could not be linked to the corrosive environment.

3.1.3 Quantification of absorbed hydrogen in bearings exposed to artificial corrosive environments

The presence of hydrogen in the steel could be originated from various sources. The dynamics of the formation of the corrosion product leads to different amounts of absorbed hydrogen in the metal at different timings. In the present work, the corrosion of the steel under different solutions was studied, from 3 to 18 days of exposure in 3-day intervals. The contribution of below mentioned solution was determined:

- pH 1.5 H_2SO_4
- pH 3.5 H_2SO_4
- pH 7 0.1 M NaCl
- pH 7 0.6 M NaCl

All results correspond to polished material, where the corrosion product was removed to analyze only the hydrogen that stays in the bulk. The surface was cleared until no visual signs of corrosion was anymore detected. To ensure consistency, three measurements under identical conditions were conducted.

The results from the exposure to H_2SO_4 with a pH of 1.5 are presented in (Table 9). The hydrogen results are illustrated in Figure 22. Initially, after 3 days, 1.90 ppm of hydrogen were detected which decreased to 1.24 ppm by the 9th day. Subsequently, the hydrogen concentration increased to 2.13 ppm, exceeding the acceptable limit by the 12th day, and then declined to 1.80 ppm by the end of the test. The highest SD of 0.70

was observed at this point. Overall, the hydrogen concentration exhibited a decrease from 1.90 ppm on the 3rd day to 1.80 ppm on the 18th day.

Table 9: *Hydrogen (ppm), oxygen (ppm), polished material (µm) and SD in polished samples exposed to pH 1.5 H_2SO_4. From top to bottom; Exposure time (days) (D), hydrogen (ppm) (H), oxygen (ppm) (O) and polished material (µm) (P).*

D	3	6	9	12	15	18
H	1.9 ± 0.1	1.9 ± 0.4	1.2 ± 0.0	2.1 ± 0.2	1.8 ± 0.2	1.8 ± 1.0
O	20.8 ± 5.3	19.5 ± 6.6	28.3 ± 7.3	36.5 ± 5.4	34.9 ± 11.1	23.4 ± 13.1
P	38 ± 3.5	48 ± 20.9	81 ± 17.9	49 ± 10.1	134 ± 89.4	63 ± 19.2

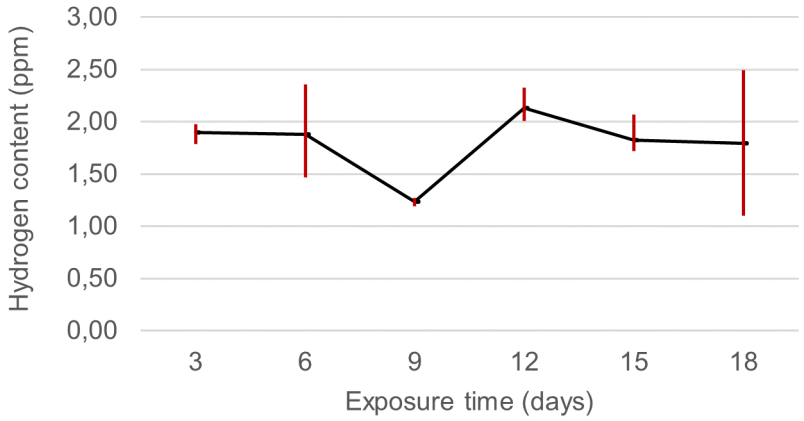

Figure 22: *Hydrogen (ppm) vs. exposure time (days) and corresponding deviation in polished samples exposed to pH 1.5 H_2SO_4.*

From samples exposed to pH 3.5 H_2SO_4 the results in Table 10 are obtained. The hydrogen concentration initially rises from 1.26 ppm to 1.39 ppm by the 9th day, followed by a decline to 0.84 ppm on the 15 th day. A subsequent increase is observed on the 18th day. Furthermore, as observed in pH 1.5 H_2SO_4, the absorbed hydrogen decreases from the initial value of 1.28 ppm to 1.08 ppm at the end of the test. These results are visually represented in Figure 23.

Table 10: *Hydrogen (ppm), oxygen (ppm), polished material (µm) and SD in polished samples exposed to pH 3.5 H_2SO_4. From top to bottom; Exposure time (days) (D), hydrogen (ppm) (H), oxygen (ppm) (O) and polished material (µm) (P).*

D	3	6	9	12	15	18
H	1.3 + 0.5	1.4 + 0.3	1.4 + 0.0	1.1 + 0.2	0.8 + 0.4	1.0 + 0.0
O	12.8 ± 3.1	10.9 ± 5.2	11.3 ± 1.8	11.7 ± 0.4	6.7 ± 1.0	27.4 ± 12.5
P	35 ± 13.4	14 ± 7.3	17 + 8.0	34 ± 9.4	27 ± 12.5	61 ± 28.1

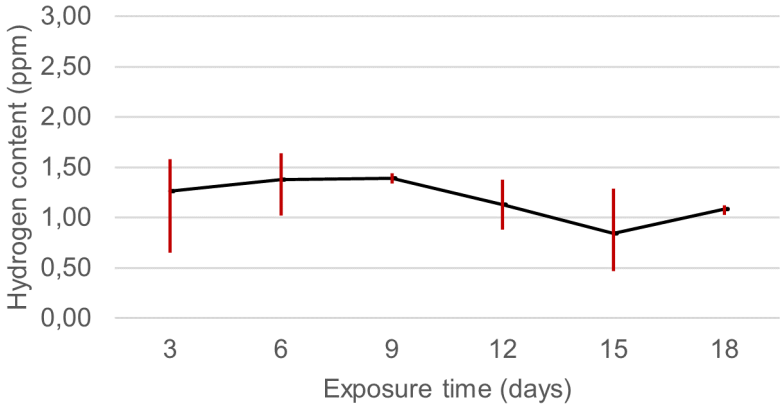

Figure 23: *Hydrogen (ppm) vs. exposure time (days) and corresponding deviation in polished samples exposed to pH 3.5 H_2SO_4.*

A comparable trend was observed in both H_2SO_4 solutions, where hydrogen initially slightly increased or remained stable before a noticeable decrease. This decrease was always followed by an increase in hydrogen. Interestingly, the minimum amount of hydrogen was not observed at the beginning, but rather during the course of the test. The significant decrease was noted between days 6 and 9 under pH 1.5, and between days 9 and 15 under pH 3.5, indicating an accelerated process under the more acidic solution. Furthermore, both cases exhibited lower levels of hydrogen at the end of the test as compared to the initial values, implying a higher rate of hydrogen absorption during the initial period. In contrast to pH 1.5, none of the results exceeded the 2 ppm limit under pH 3.5.

In a pH 7 0.1 M NaCl solution, a significant initial increase in hydrogen was observed up to the 9th day, from 1.36 to 2.79 ppm, Table 11. This was followed by a decrease to 1.48 ppm by the 15th day, and a final increase to 2.62 ppm. Similar to the observations made in the pH 1.5 H_2SO_4 solution, some of the values again exceeded the 2 ppm limit. The initial hydrogen content of 1.36 ppm on the 3rd day increased significantly to 2.62 ppm by the 18th day. This is illustrated in Figure 24.

Table 11: *Hydrogen (ppm), oxygen (ppm), polished material (µm) and SD in polished samples exposed to pH 7 0.1 M NaCl. From top to bottom; Exposure time (days) (D), hydrogen (ppm) (H), oxygen (ppm) (O) and polished material (µm) (P).*

D	3	6	9	12	15	18
F	1.4 ± 0.4	2.1 ± 0.7	2.8 ± 0.9	2.6 ± 0.5	1.5 ± 0.7	2.6 ± 0.9
O	26.6 ± 4.4	13.7 ± 4.2	54.6 ± 50.7	14.9 ± 10.3	26.4 ± 23.9	12.2 ± 4.6
P	371 ± 212.6	415 ± 84.4	307 ± 97.9	474 ± 153.9	683 ± 35.1	384 ± 123.5

To identify the most vulnerable environmental condition to hydrogen-assisted damage, an additional corrosive solution was investigated. A pH 7 NaCl solution with a

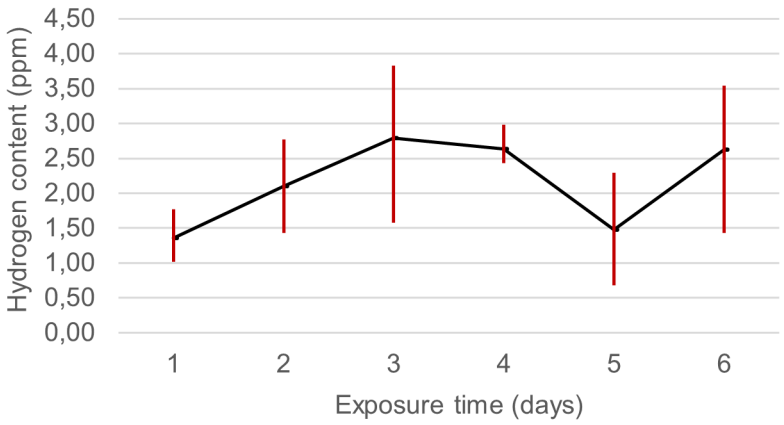

Figure 24: *Hydrogen (ppm) vs. exposure time (days) and corresponding deviation in polished samples exposed to pH 7 0.1 M NaCl.*

molarity of 0.6 was chosen for this purpose. The hydrogen and oxygen concentration, the removed material (µm), and SD are presented in Table 12, illustrated in Figure 25. Hydrogen content is very constant, unlike in previous solutions where certain trends were visible. Moreover, the lowest hydrogen concentrations were analyzed, from 0.76 ppm the third day to a maximum of 1.08 ppm the 15th day, and a final concentration of 0.97 ppm the 18th day.

Table 12: *Hydrogen (ppm), oxygen (ppm), polished material (µm) and SD in polished samples exposed to pH 7 0.6 M NaCl. From top to bottom; Exposure time (days) (D), hydrogen (ppm) (H), oxygen (ppm) (O) and polished material (µm) (P).*

D	3	6	9	12	15	18
H	0.8 ± 0.2	0.8 ± 0.2	0.9 ± 0.3	0.8 ± 0.1	1.1 ± 0.3	1.0 ± 0.2
O	2.3 ± 0.8	9.0 ± 11.8	2.3 ± 2.0	11.1 ± 0.9	13.0 ± 13.3	17.9 ± 12.6
P	209 + 26.6	593 ± 80.2	442 ± 254.3	696 ± 141.3	776 ± 200.9	817 ± 66.0

Higher absorbed hydrogen was detected in pH 7 0.1 M NaCl, followed by pH 1.5 H_2SO_4. These are the only two environments overcoming the established 2 ppm limit. pH 3.5 H_2SO_4 and pH 7 0.6 M NaCl overlap each other, with an initial higher hydrogen under pH 3.5 H_2SO_4 that end up leveling.

The hydrogen in the bulk and removed material were tried to be linked. However no significant relationship could be established. The amount of polished material needed for a clean surface was much less in H_2SO_4 solutions than in NaCl. This is visible in Figure 26 where the polished material is illustrated with respect to the exposure time for the four environments. In H_2SO_4 a maximum of 134 µm were polished for a clean surface, while under NaCl was up to 818 µm. The only corrosive environment that indicates a linear growth of the product is 0.6 M NaCl. The rest show noticeable variations

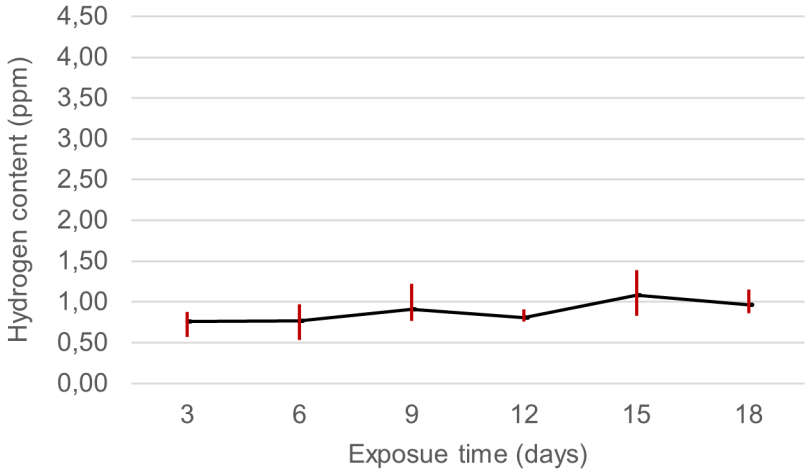

Figure 25: *Hydrogen (ppm) vs. exposure time (days) and corresponding deviation in polished samples exposed to pH 7 0.6 M NaCl.*

with time in the amount of material removed.

The formed product was often very irregular, mainly in NaCl solutions. The technique used for the heigh measurements and product growth study was not ideal. This was based on single point measurements, which could not cover the morphology of the rust over the surface. This is probably the reason why no relationship could be established. Moreover, the manual polishing makes it difficult to maintain the removed material constant throughout the study. This should be studied by using other techniques in future works.

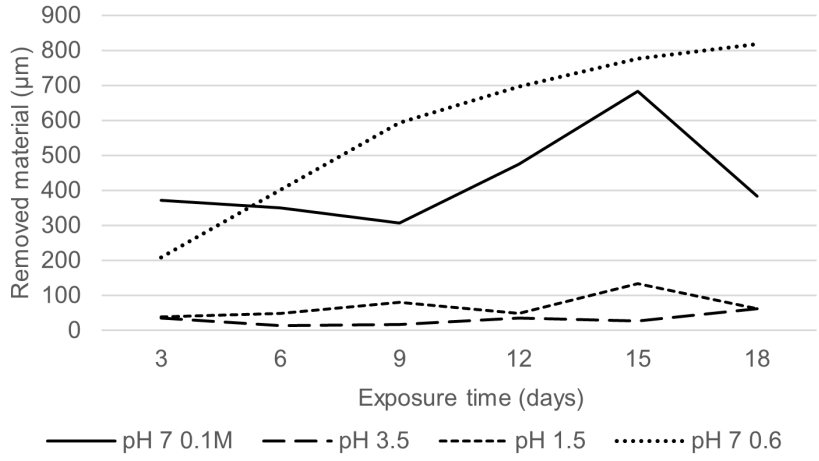

Figure 26: *Polished material (µm) vs. exposure time (and) and corresponding deviation in polished samples exposed to pH 1.5 H_2SO_4, pH 3.5 H_2SO_4, pH 7 0.1 M NaCl and pH 7 0.6 M NaCl.*

3.1.4 The influence of the polished surface on the hydrogen absorption when exposed to corrosion

To investigate the correlation between the surface roughness and the hydrogen absorption behavior, the samples were subjected to polishing prior to their exposure. This technique is described as METHOD 2 in (Reference). Previously, for the simulation of in-field service, samples were only cleaned before being placed in the chamber. This time samples were pre-polished, and the newly generated surface was exposed to the aggressive environment. The solutions applied were again pH 1.5 H_2SO_4 , pH 3.5 H_2SO_4, pH 7 0.1 M NaCl, and pH 7 0.6 M NaCl. After exposure, same procedure was repeated. The surface was manually polished until obtaining a clean surface, and the hydrogen was measured. The aim of the study was to determine whether the newly generated polished surface has an impact on the hydrogen absorption.

The hydrogen concentration in samples that underwent polishing prior to exposure to corrosive media is lower than those samples that were not polished. The graphical representation of this finding can be observed in Figure 27. It is noteworthy that none of the samples surpassed the established threshold of 2 ppm, in contrast to the outcomes of previous experiments. Furthermore, both hydrogen and oxygen (Figure 28)levels displayed greater stability over the duration of the exposure period. However, the amount of removed material show similar trends as before, where pH 7 NaCl solutions need more polishing that H_2SO_4 solutions, Figure 29.

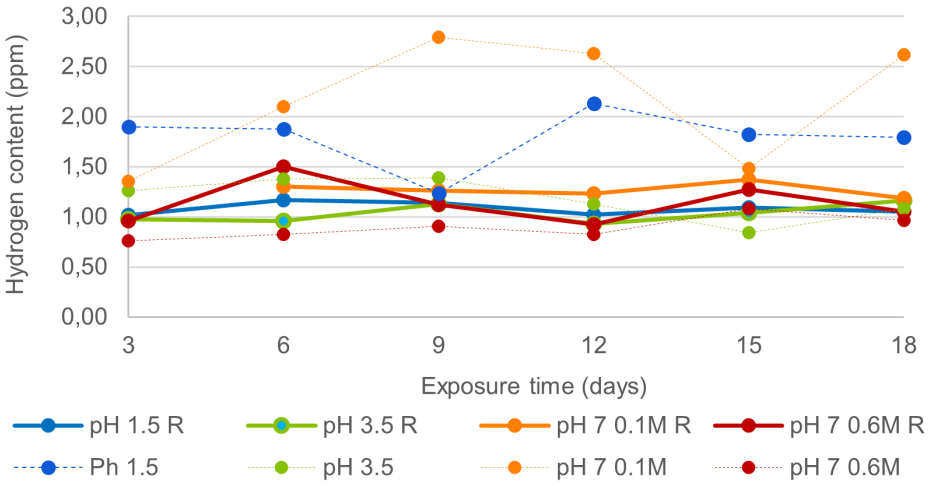

Figure 27: *Hydrogen (ppm) vs. exposure time under pH 1.5 H_2SO_4, pH 3.5 H_2SO_4, pH 7 0.1 M NaCl and pH 7 0.6 M NaCl in samples polished before exposure corrosion (R), and non-polished before exposure.*

The reduction in the scatter of hydrogen and oxygen observed in the polished samples can be attributed to the removal of hydrogen storage sites during the polishing

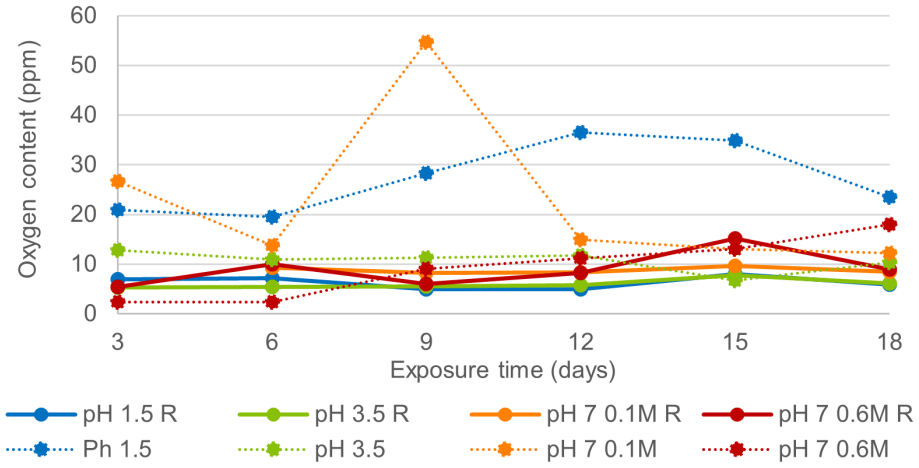

Figure 28: *Oxygen (ppm) vs. exposure time under pH 1.5 H_2SO_4, pH 3.5 H_2SO_4, pH 7 0.1 M NaCl and pH 7 0.6 M NaCl in samples polished before exposure corrosion (R), and non-polished before exposure.*

process. This process effectively decreases the number of surface sites available for hydrogen trapping, which in turn mitigates hydrogen accumulation within the material. The presence of surface traps such as small pits and scratches are expected in the non-corroded bearing. Additionally, the polishing process can create a more uniform surface, which reduces the likelihood of localized corrosion.

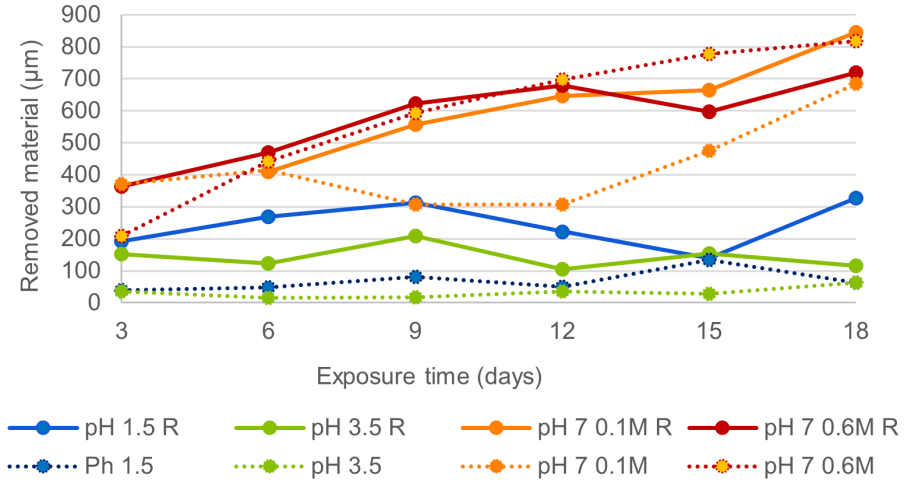

Figure 29: *Removed material (µm) vs. exposure time under pH 1.5 H_2SO_4, pH 3.5 H_2SO_4, pH 7 0.1 M NaCl and pH 7 0.6 M NaCl in samples polished before exposure corrosion (R), and non-polished before exposure.*

3.2 Characterization of absorbed hydrogen based on trapping and desorption analysis

The hydrogen concentration under different environments was previously defined by MET. This was followed by the Thermal Desorption Spectroscopy (TDS) technique, employed to investigate the mechanism of hydrogen desorption, and to characterize the hydrogen traps in the microstructure. The methodology used for the determination of the desorbed hydrogen was outlined in Chapter 2, Materials and Methods , where calibration was taken into account. This procedure is repeated for the analysis of all subsequent results. In order to ensure the reliability of the findings and make solid conclusions, various measurements were carried out for each test condition. All tests are concurrently displayed in the graphical representations of the results.

In the TDA the positioning of the peak indicates the binding energy of the hydrogen to the metal lattice. Peaks visible at higher temperatures correspond to hydrogen that is more strongly trapped, while at lower temperatures the activation energy for hydrogen to leave the site is less. The TDS allows the study of the hydrogen-metal interaction, where the presence of various peaks represent different types of hydrogen in the material. The obtained spectrum consists of different desorption peaks originating each from a trap site releasing the hydrogen stored. The desorption spectrum comprises distinct and overlapping peaks from the numerous possible trap sites in the metal microstructure.

The method applied heats the sample from 27 °C to 400 °C in a 5 °C /min. The peaks over this temperature are not considered, limiting the study to hydrogen that is reversibly trapped in the material.

3.2.1 Trapping behavior of hydrogen in the as received non-corroded bearing

The spectra obtained from the TDS analysis of the non-corroded bearing samples did not exhibit any peaks, suggesting that the hydrogen content detected is accumulated in deeper traps with higher binding energy. The current method, where samples are heated up to 400 °C, is not enough for the desorption of the hydrogen. Consequently, the hydrogen detected in MET technique corresponds to more deeply trapped hydrogen.

3.2.2 Trapping behavior of hydrogen in the as received bearing corroded in P&P industry

The as received corroded bearing from pulp and paper industry revealed that no hydrogen desorption happened in either non-polished or polished samples from the raceway (CL and CR). In contrast, desorption peaks were detected in non-polished samples from the middle zone (CM). The temperature of the single peak is located around 200 °C to 300 °C Figure 30. A smaller peak at over 400 °C was also observed, which can be attributed to hydrogen trapped in a complex with other elements, such as carbides or oxides. This is likely due to the presence of some corrosion product remaining on the surface, which may contain hydrogen storage sites not considered in this study. The polished CM samples exhibited negligible or no hydrogen, suggesting that the reversible hydrogen was entirely removed by the polishing process.

Table 13: *Desorbed hydrogen (ppm) and removed material (µm) of the corroded front middle zone (CM).*

Sample / zone	Hydrogen (ppm)	Removed material (µm)
Corroded middle non-polished (CM)	0.2 ± 0.2	0
Corroded middle polished (CM)	-	40.7 ± 28.4

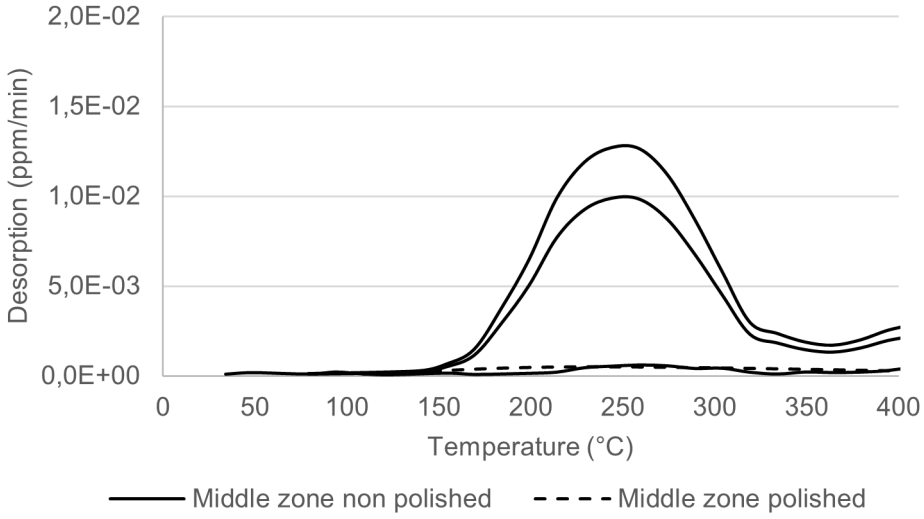

Figure 30: *Hydrogen desorption rate (ppm/min) vs temperature (°C) in corroded front middle zone (CM).*

More pronounced hydrogen peaks were observed in the surface in contact with the shaft (CBK). Figure 31 illustrates the spectra obtained from non-polished and polished samples of CBK1, the zone with most visible corrosion. Non-polished samples again

exhibited a single prominent desorption peak coming out of the spectra. This peak exceeds the 400 °C temperature range considered in the present study, and is again linked to the hydrogen in the surface corrosion layer. Meanwhile polished samples again displayed minimal or no desorption of hydrogen.

Table 14: *Desorbed hydrogen (ppm) and removed material (µm) from corroded Back Zone 1 (CBK1).*

Sample / zone	Hydrogen (ppm)	Removed material (µm)
Corroded middle non-polished (CM)	0.3 ± 0.2	0
Corroded middle polished (CM)	-	133 ± 39.8

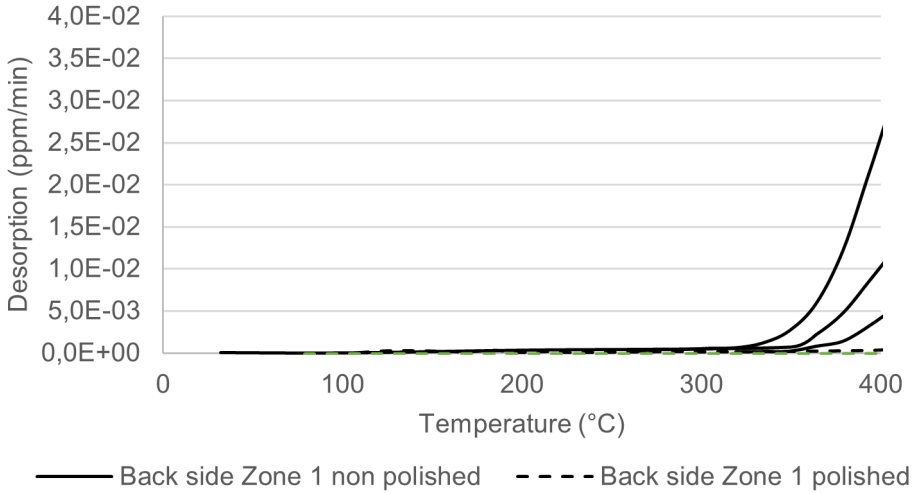

Figure 31: *Hydrogen desorption rate (ppm/min) vs temperature (°C) in corroded Back Zone 1 (CBK1).*

3.2.3 Trapping behavior of hydrogen in bearings exposed to artificial corrosive environments

The investigation of trapping of hydrogen was also conducted in extreme environments. The aim was to determine if the type of corrosive media potentially impacts the trapping behavior, as it was observed with the quantities absorbed in MET measurements. The diffusivity of hydrogen was also tried to be understood. Unlike in bearings obtained from Steyr, the material is now charged, polished and immediately measured. This is of particular significance as, in practical applications bearings are not typically used immediately after remanufacturing. Therefore, understanding the behavior of hydrogen during exposure following remanufacturing is also important.

Two situations were considered to investigate the behavior of hydrogen after remanufacturing. The first involved taking samples out of the chamber, polishing, and measuring immediately. This estimates the total hydrogen content in the sample. The second test analyzed the behavior of hydrogen after 24 h of exposure at room temperature. Samples were taken out, immediately polished, and measured 24 h after the polishing. This estimates the amount of hydrogen trapped by reversible traps, by detecting the hydrogen that left the sample during this time. The hydrogen that leaves the material is categorized as diffusible hydrogen.

The diffusible hydrogen in samples charged in H_2SO_4 was less in the most acidic environment, pH 1.5. Initially, hydrogen was placed not in a single feature but in various with varying trapping energies seen in Figure 32. After 24 h at room temperature, part of the hydrogen diffused out, and the rest diffuses towards other trapping sites at higher binding energies. Initially the peaks are located between 50 °C and 200 °C, and shift towards 150 to 250 °C range. Moreover, the peak morphology changes into a single peak, indicating the accumulation of hydrogen in a specific feature. It is important to consider that very low reversible hydrogen contents are being detected, Table 15, and therefore the obtained noticeable difference between peaks.

Table 15: *Desorbed hydrogen (ppm) and removed material (µm) in polished samples exposed to pH 1.5 H_2SO_4 for 9 days; taken out from the chamber, polished and measured immediately (polished), and measured 24h after (prepolished).*

Sample / zone	Hydrogen (ppm)	Removed material (µm)
pH 1.5 H_2SO_4 for 9 days –immediately after polishing	0.02 ± 0.00	182 ± 13.9
pH 1.5 H_2SO_4 for 9 days – 24h later polishing	0.01 ± 0.01	197 ± 15.6

Due to technical complications with the TDS, it was unfeasible to conduct tests for the 18-day exposure to the pH 1.5 H_2SO_4 corrosive medium. Consequently, the outcomes obtained from the 9th day of exposure will be solely used for comparative purposes against other corrosive media.

Under pH 3.5 a higher concentration of reversible hydrogen is observed, Figure 33, in a single peak at 175 - 250 °C. However, after 24 hours of exposure at room temperature all the diffusible hydrogen is released from the material, Table 16. When exposed for 18 days, less diffusible hydrogen is recognized, at slightly lower binding energies, but most of it stays in the material after 24h at slightly higher peak temperatures. This is stored at different trapping sites, recognized by the presence of different peaks, Figure 34. The desorption of hydrogen after 9 days of charging can be due to how deep the hydrogen

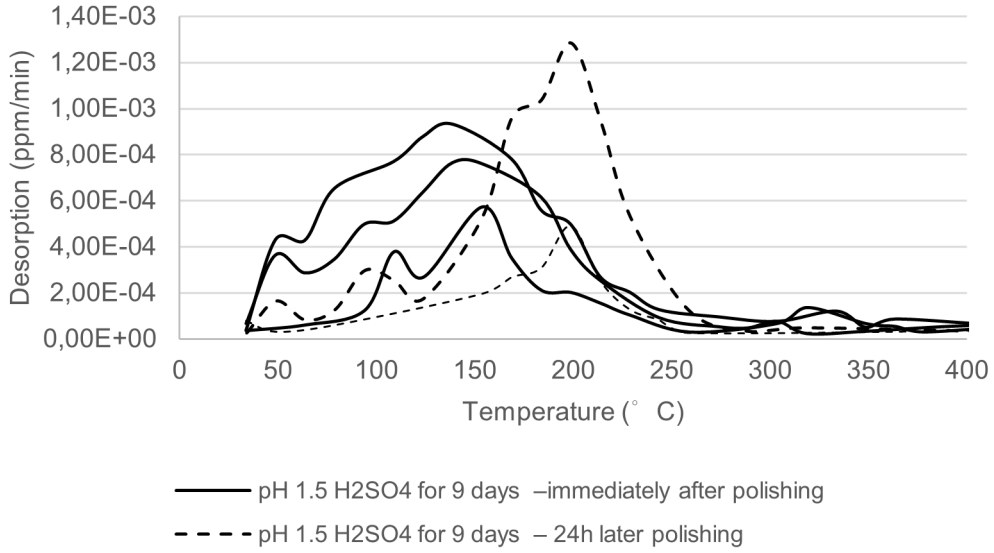

Figure 32: *Hydrogen desorption rate (ppm/min) vs temperature (°C) in polished samples exposed to pH 1.5 H_2SO_4 for 9 days; taken out from the chamber, polished and measured immediately (polished), and measured 24h after (prepolished).*

is in the material. Compared to 18 days of charging, the hydrogen has diffused a lower distance through the bulk and is more easily desorbed.

Table 16: *Desorbed hydrogen (ppm) and removed material (µm) in polished samples exposed to pH 3.5 H_2SO_4 for 9 and 18 days; taken out from the chamber, polished and measured immediately (polished), and measured 24h after (prepolished).*

Sample / zone	Hydrogen (ppm)	Removed material (µm)
pH 3.5 H_2SO_4 for 9 days –immediately after polishing	0.12 ± 0.06	18 2± 11.5
pH 3.5 H_2SO_4 for 9 days – 24h later polishing	-	149 ± 10.8
pH 3.5 H_2SO_4 for 18 days –immediately after polishing	0.04 ± 0.03	128 ± 35.4
pH 3.5 H_2SO_4 for 18 days – 24h later polishing	0.01 ± 0.01	162 ± 34.8

In samples exposed to NaCl, diffusion of hydrogen at room temperature is observed to happen faster. In every test, the first measurement immediately after charging (30 min after being taken out from the chamber) show more hydrogen than the other subsequent tests (90 min and 180 min). Therefore 2 h exposure to room temperature at ambient conditions is enough to desorb some of the diffusible hydrogen in the steel.

In 0.1 M NaCl, diffusible hydrogen slightly increases with exposure time, shifting towards lower temperatures, Figure 35 and Figure 36. In the 24 h at room temperature,

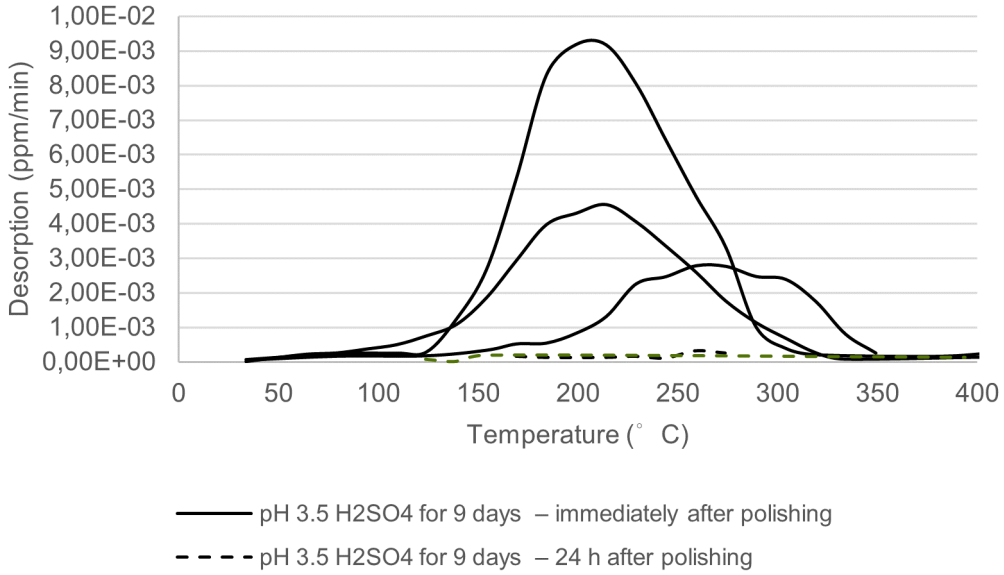

Figure 33: *Hydrogen desorption rate (ppm/min) vs temperature (°C) in polished samples exposed to pH 3.5 H_2SO_4 for 9 days; taken out from the chamber, polished and measured immediately (polished), and measured 24h after (prepolished).*

diffusible hydrogen absorbed during the first 9 days stays constant with a slight redistribution, while after 18 days, most of it is desorbed, Table 17. In day 9 a considerable increase of hydrogen is observed after 24 h. This was concluded to be due to the formation of an oxide film among the 24 h were the newly generated surface reacts with the environment. Th formation of this oxide film is considered an experimental error, and therefore is not considered as does not represent the hydrogen in the bulk.

Table 17: *Desorbed hydrogen (ppm) and removed material (µm) in polished samples exposed to pH 7 0.1 M NaCl for 9 and 18 days; taken out from the chamber, polished and measured immediately (polished), and measured 24h after (prepolished).*

Sample / zone	Hydrogen (ppm)	Removed material (µm)
pH 7 0.1 M NaCl for 9 days – immediately after polishing	0.06 ± 0.03	378 ± 21.8
pH 7 0.1 M NaCl for 9 days – 24h later polishing	0.15 ± 0.04	358 ± 75.6
pH 7 0.1 M NaCl for 18 days –immediately after polishing	0.17 ± 0.08	580 ± 71.3
pH 7 0.1 M NaCl for 18 days – 24h later polishing	0.01 ± 0.0	828 ± 163.3

The highest diffusible hydrogen is found in 0.6 M NaCl environments, with similar contents after 9 and 18 days of exposure, located at the same features throughout the exposure of the material, Figure 38. Most of it leaves the material at room temperature, Table 18, with a slight peak shift to higher temperatures in samples exposed for 9 days,

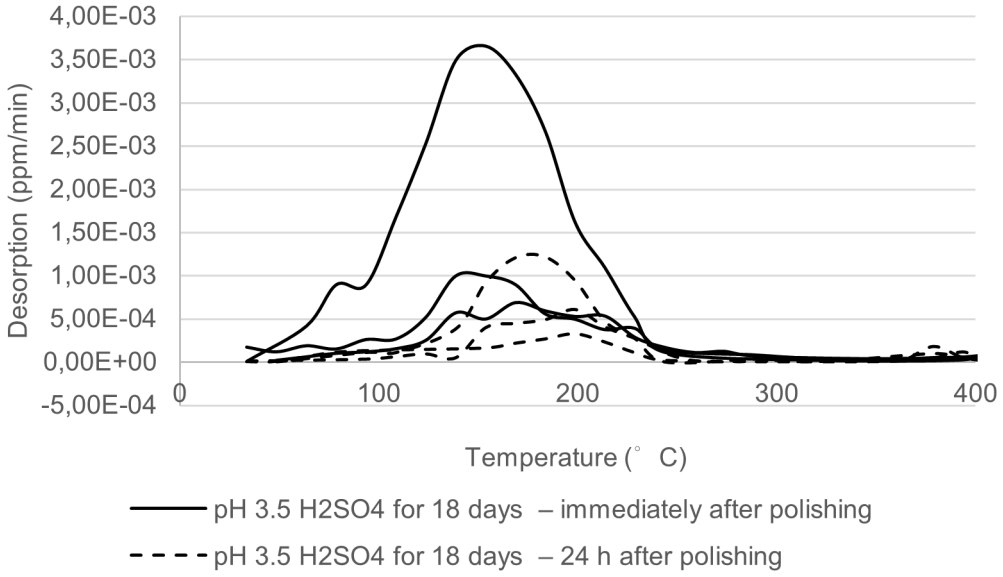

Figure 34: *Hydrogen desorption rate (ppm/min) vs temperature (°C) in polished samples exposed to pH 3.5 H_2SO_4 for 18 days; taken out from the chamber, polished and measured immediately (polished), and measured 24h after (prepolished).*

Figure 37.

Table 18: *Desorbed hydrogen (ppm) and removed material (µm) in polished samples exposed to pH 7 0.6 M NaCl for 9 and 18 days; taken out from the chamber, polished and measured immediately (polished), and measured 24h after (prepolished).*

Sample / zone	Hydrogen (ppm)	Removed material (µm)
pH 7 0.6 M NaCl for 9 days – immediately after polishing	0.10 ± 0.10	462 ± 105.1
pH 7 0.6 M NaCl for 9 days – 24h later polishing	0.01 ± 0.01	359 ± 120.7
pH 7 0.6 M NaCl for 18 days –immediately after polishing	0.25 ± 0.09	772 ± 139.4

To summarize, the highest amount of reversible hydrogen after 9 days was found in the following order:

$$\text{pH 7 0.6M NaCl} > \text{pH 7 0.1M NaCl} > \text{pH 3.5 } H_2SO_4 > \text{pH 1.5 } H_2SO_4$$

environments containing NaCl containing higher levels of reversible hydrogen. On the other hand, solutions with lower pH values show more hydrogen trapped at irreversible sites in the material. The peak positions were arranged in the following order:

$$\text{pH 7 0.6M NaCl} = \text{pH 1.5 } H_2SO_4 > \text{pH 7 0.1M NaCl} > \text{pH 3.5 } H_2SO_4$$

The amount of diffusible hydrogen was similar at longer exposure times:

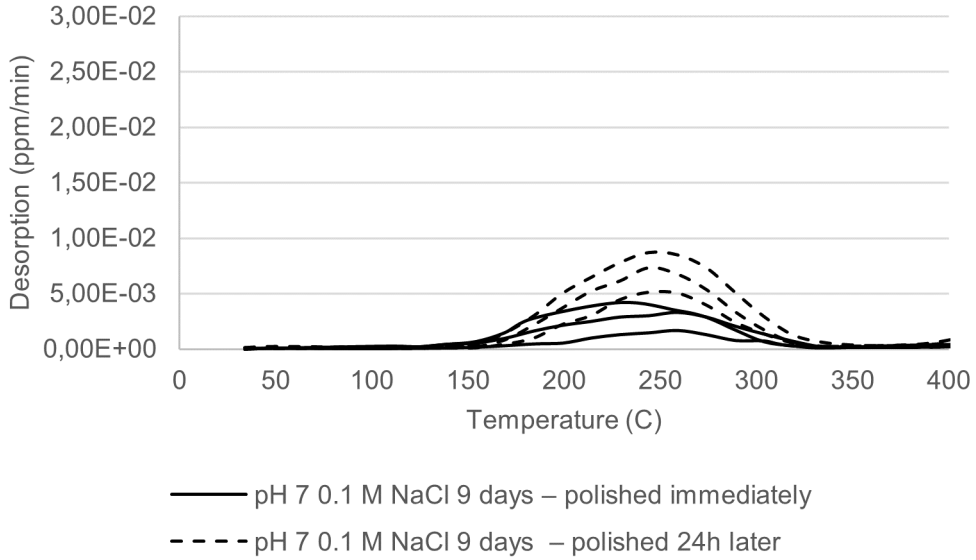

Figure 35: *Hydrogen desorption rate (ppm/min) vs temperature (°C) in polished samples exposed to pH 7 0.1 M NaCl for 9 days; taken out from the chamber, polished and measured immediately (polished), and measured 24h after (prepolished).*

$$\text{pH 7 0.6M NaCl} > \text{pH 7 0.1M NaCl} > \text{pH 3.5 } H_2SO_4$$

The results reveal an increasing reversible hydrogen with exposure time in both NaCl solutions, and a decrease in pH 3.5 H_2SO_4. At longer exposure times, the main peaks of diffusible hydrogen were placed in the same position, suggesting the accumulation of hydrogen in a specific site. Notably, the peaks at higher binding energies (pH 3.5 H_2SO_4 and pH 7 0.1M NaCl) exhibited a shift towards lower peak temperatures. The peak positions were as follows:

$$\text{pH 7 0.6M NaCl} = \text{pH 7 0.1M NaCl} = \text{pH 3.5 } H_2SO_4$$

The amount of diffusible hydrogen in the most acidic environments was less, which in turn decreases the likelihood of hydrogen-enhanced damages.

3.2.4 Signal interpretation

It was observed that both the exposure time and the corrosive media significantly influence the distribution and trapping of hydrogen in the material. However, it is still complex to address the distribution and behavior. Several procedures are used to obtain the desorption energy related to a specific trap, but defining a method to separate the different peaks is still challenging.

The hydrogen desorption process and the energy required for the hydrogen to leave the traps can be determined by comparing a material's spectra at different heating

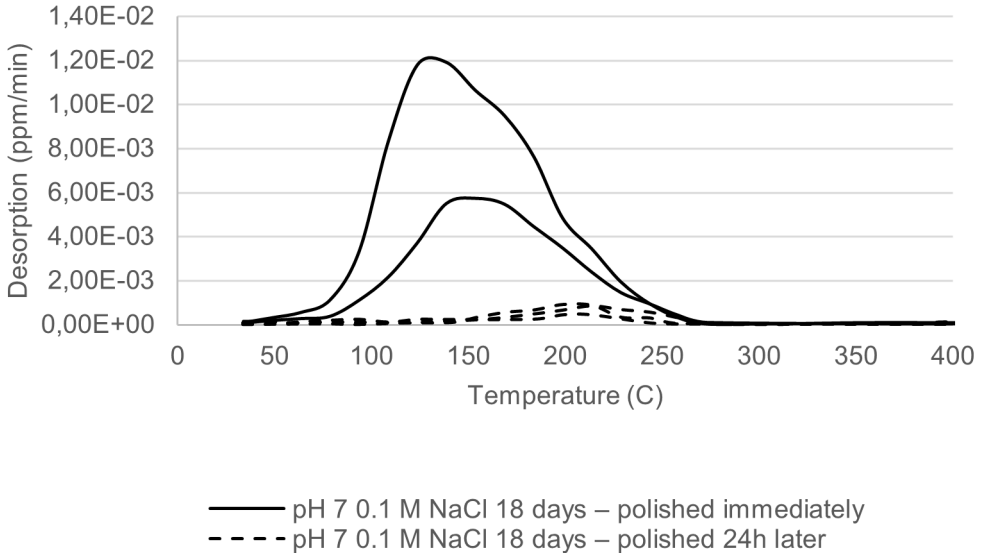

Figure 36: *Hydrogen desorption rate (ppm/min) vs temperature (°C) in polished samples exposed to pH 7 0.1 M NaCl for 18 days; taken out from the chamber, polished and measured immediately (polished), and measured 24h after (prepolished).*

rates. Though the variation of the method and the heating rate applied, desorption peaks shift, and the trap activation energy is determined from the change in the peak temperature [1]. For this, the different desorption peaks need to be individually characterized. The hydrogen released from the trap has a Gaussian distribution, which form the spectrum by the combination a given number of Gaussian peaks that overlap. Each curve represents an absorption site in the steel and need to be fitted in the obtained spectra.

The complexities of deconvoluting a TDS spectrum reside in the possible different fittings which would fill in the spectrum at different activation energies and frequencies. There are publications that collect thermodynamic kinetics of diffusion and desorption processes, such as the one published by Pressouyre [21], that clasify the hydrogen traps in steel according to their size. However, these are characteristic of each material as the peaks are dependent on the metallurgical microstructures of steels, and cannot always be combined with experimental data. These are mainly relatable when studying the hydrogen behavior in a reference material under different conditions. In the presence work, the lack of information about the desorption rate, temperature, and the interacting activation energy of hydrogen in traps in the analyzed material, does not allow the determination of detailed hydrogen location. Further investigation is needed to determine the hydrogen trap corresponding to each temperature peak. Moreover, the complexity of the data interpretation often makes it hard to distinguish between the hydrogen desorption of various trap sites that release hydrogen in the same tempera-

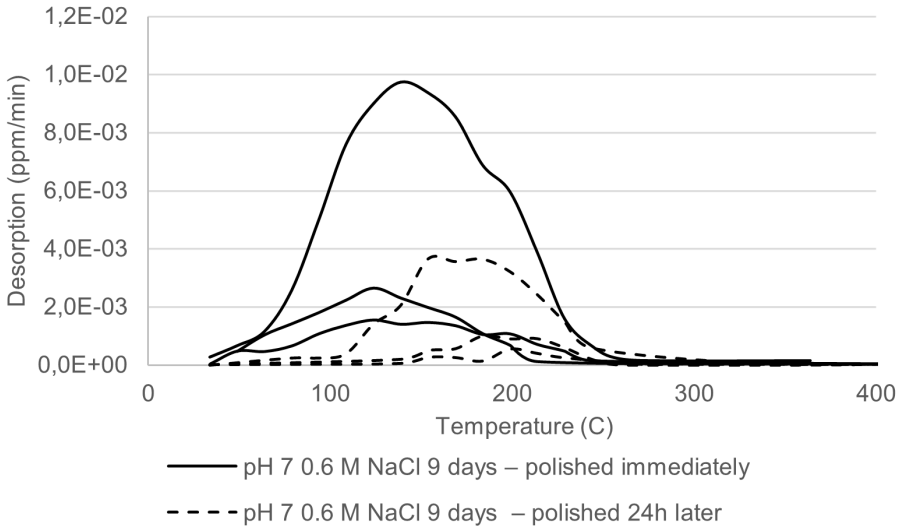

Figure 37: *Hydrogen desorption rate (ppm/min) vs temperature (°C) in polished samples exposed to pH 7 0.6 M NaCl for 9 days; taken out from the chamber, polished and measured immediately (polished), and measured 24h after (prepolished).*

ture region. For this, other complementary techniques should be used. It is beyond the scope of this work to discuss these techniques.

The results show very low-intensity peaks, where the observed tendencies were quite clear but displayed some scatter in the measurements, even in samples exposed to the same condition. Studies have shown that the scatter in hydrogen subsurface concentrations can be an order of magnitude even when using identical charging conditions [turk2018grain]. This is intensified if minimal hydrogen contents are considered, as in the present work. Some experimental scatter is thus inevitable. Moreover, the analyzed steel already showed some hydrogen accumulation in previous results from the reference material. This hydrogen is again expected to be found and can influence the outcome.

Moreover, the TDS is a thermal destructive technique, which can cause alterations in the microscopic characteristics of the steel during the heating cycle [verbeken2012analysing]. The obtained signal can be due to a trap site releasing its hydrogen or due to a trap site being altered or annihilated. Additional techniques should be used for a complete interpretation.

3.3 Influence of the corrosion product buildup on the hydrogen absorption

After the hydrogen quantification, the observed quantities, behavior and trends were tried to relate to the formation and dynamics of the corrosion product. For this a

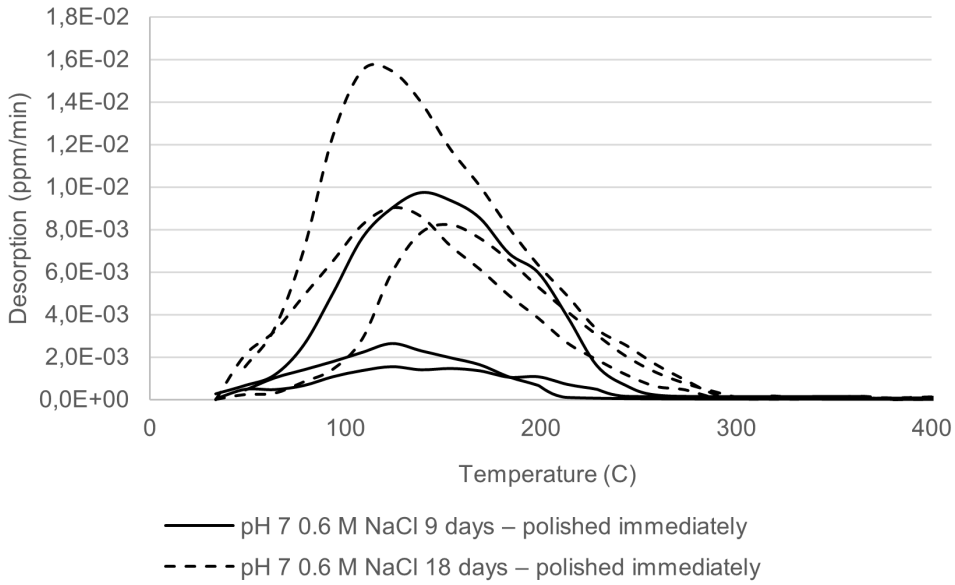

Figure 38: *Hydrogen desorption rate (ppm/min) vs temperature (°C) in polished samples exposed to pH 7 0.6 M NaCl for 9 and 18 days; taken out from the chamber, polished and measured immediately (polished), and measured 24h after (prepolished).*

closer examination was conducted on the product formed on the surface exposed to the different environments.

3.3.1 Surface analysis of the as received non-corroded bearing

Despite its non-corroded status, the reference bearing displayed minor pits in the raceway, as illustrated in Figure 39. These corrosion pits could be responsible of the hydrogen content overcoming the 2ppm, displayed in Table 5. These are not easily recognized by the human eye due to their small size (µm scale) and therefore a visual inspection could not be enough to address their presence.

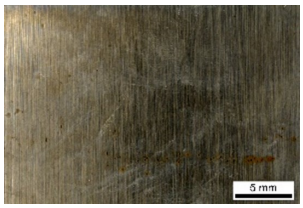

(a) Non corroded zone A

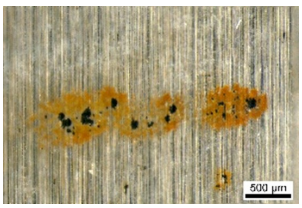

(b) Pits at non corroded zone A

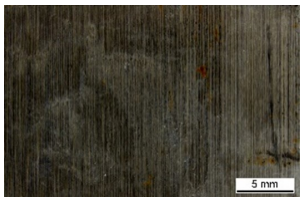

(c) Non corroded zone B

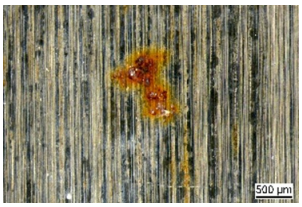

(d) Pits at non corroded zone B

Figure 39: OM images of pits found in the raceway of the non-corroded/reference segment. Two different locations (top and bottom) where corrosion pits are found. On the right a closer look of these pits is shown.

3.3.2 Surface analysis of the as received bearing corroded in P&P industry

For the inspection of the as received corroded bearing the raceway was divided based on the location as Illustrated in Figure 3.3; CL, CM and CR (left, middle and right). The back side in contact with the shaft was divided based on the degree of corrosion; CBK1, CBK2 and CBK3 (being CBK1 the most corroded). In CL and CR no corrosion product covered the surface. However, some pits were found in a µm scale, probably due to contact during the application, Figure 40. Most noticeable pits and nucleation sites were recognized in CR, Figure 41. In CM a wear mark is visible, Figure 42, suggesting that the bearing was in contact with another surface before. The specific cause of the mark cannot be determined with certainty. It may have resulted from contact during application or storage of the bearing.

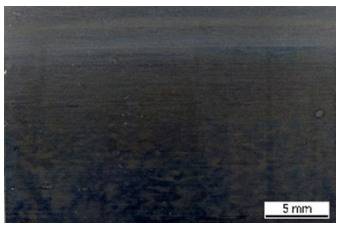

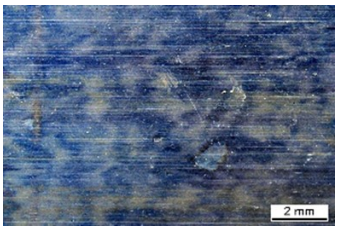

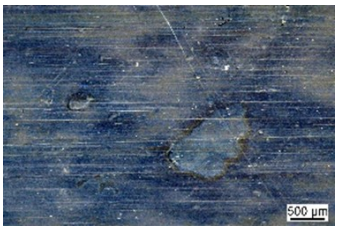

Figure 40: Left side of the raceway from the corroded bearing. The figures correspond to the same area (CL) but at different locations and focus. Small pits are visible at the surface.

The back side of the segment exhibited a significant degree of corrosion with varying levels throughout the surface. One of the corners, CBK1, notably contained most

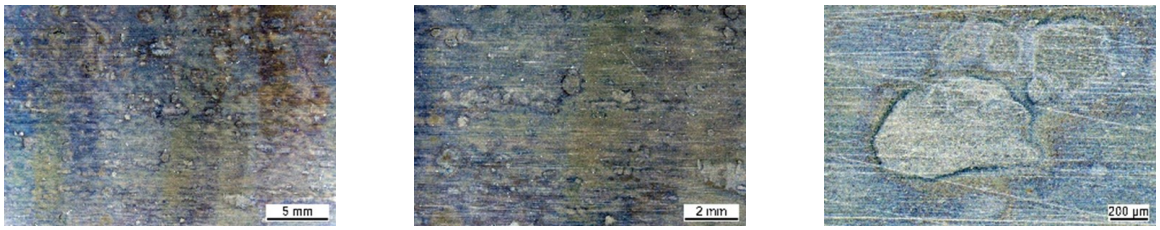

Figure 41: Right side of the raceway from the corroded bearing. The figures correspond to the same area (CR) but at different locations and focus. Small pits are visible at the surface.

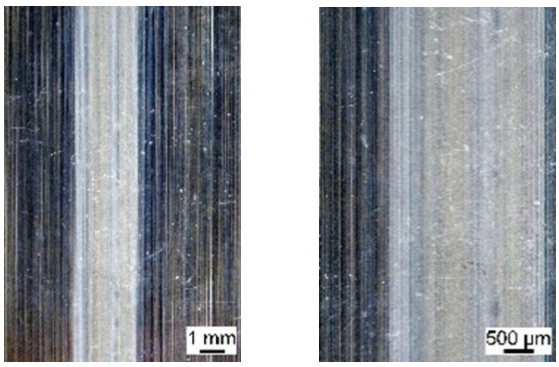

Figure 42: Middle zone of the raceway from the corroded bearing. The figures correspond to the same area (CM) but at different locationsfocus. A wear mark is visible.

corrosion product. This is observed in Figure 43 at various magnifications. The rest of the back side is less corroded, but still some corrosion product is found. Figure 44 correspond to CBK2, and Figures Figure 45 to CBK3. Little corrosion pits are also found.

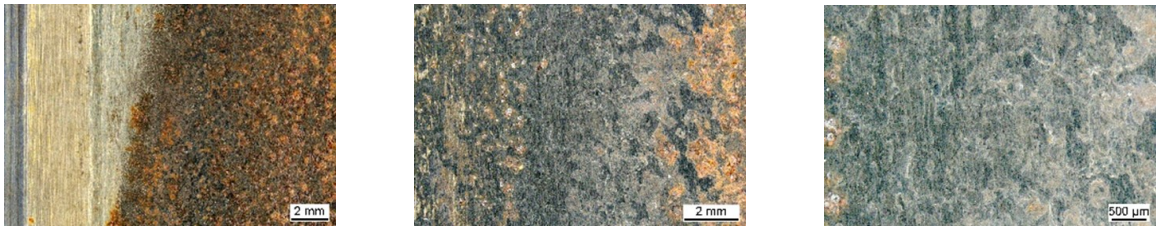

Figure 43: Corroded zone 1, CBK1 zone, in the back side of the corroded bearing.

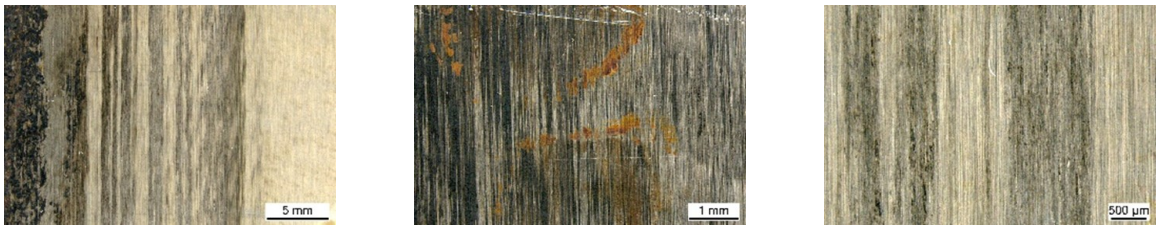

Figure 44: Corroded zone 2, CBK2 zone, in the back side of the corroded bearing.

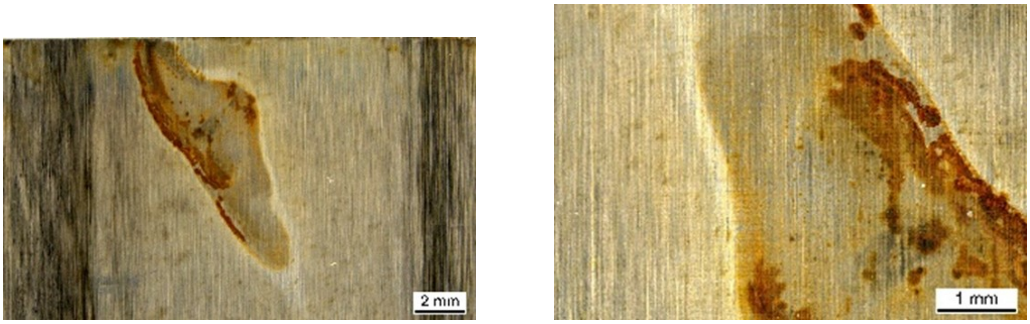

Figure 45: Corroded zone 3, CBK3 zone, in the back side of the corroded bearing.

3.3.3 Surface analysis of bearings exposed to artificial corrosive environments

SEM micrographs were taken to study the surface morphology of the samples exposed to the corrosive environments in the chamber. The corrosion product dynamics were analyzed in pH 1.5 and 3.5 H_2SO_4, and pH 7 NaCl, 0.1 and 0.6 M, over a period of 6 to 18 days. The corrosion product was observed to cover the surface within the first 72 hours (3 days), increasing the covered area with time. The microscopic morphologies revealed that the corrosion product was a complex composite of several phases formed in combination with each other and varied across different corrosive environments.

In pH 1.5 H_2SO_4, the product contains crater like shapes and numerous micro-cracks, Figure 46a. With time a more even layer covers the surface. The even surface is formed by a cross-network product with a small fine plate, flowery structure, Figure 46b, probably corresponding to γ-FeOOH (lepidocrocite). Inside the craters a more rod-like morphology is found. The flowery structure keeps growing until the 12th day covering most of the surface, while the rod shape morphology is kept in some smaller areas. Cracks keep being visible in the product due to the aggressiveness of the environment. By the 15th day the corrosion product drastically changes. The surface that contained craters transform into a more even surface with precipitates on it, Figure 46c. The even surface is formed by cotton ball structures corresponding to α-FeOOH. However, by the 18th day the crater containing surface and the flowery structure cover most of the surface again.

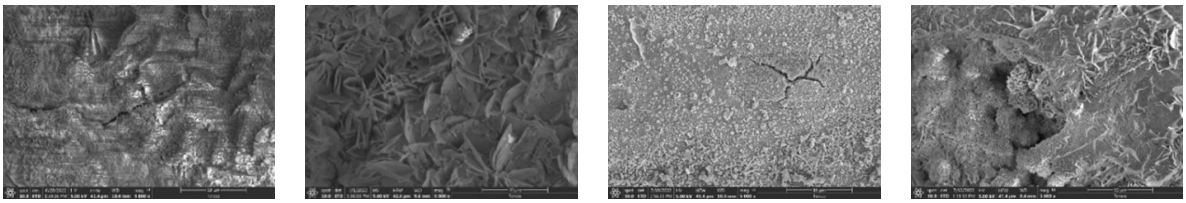

(a) 9th day x 5000 (b) 12th day x 5000 (c) 15th day x 5000 (d) 18th day x 5000

Figure 46: Corrosion product morphology of samples exposed to pH 1.5 H_2SO_4 (Exposure time and magnification).

Under pH 3.5 a similar behavior is observed. In the 9th day flowery structures are growing in an irregular manner from a more even surface with crater like shapes, Figure 47a. The product is once again mainly composed by flowery structure γ-FeOOH (Figure 47b) until the 15th day where cotton ball structures are dominant corresponding to α-FeOOH, Figure 47c. The product is spread in a more uniform way covering the surface. Flowery structures are still visible in small quantities. In the 18th day γ-FeOOH is again the main component with a similar morphology seen in day 12, Figure 47.

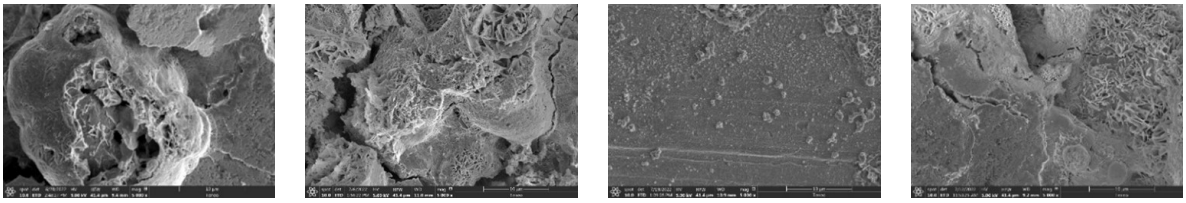

(a) 9th day x 5000 (b) 12th day x 5000 (c) 15th day x 5000 (d) 18th day x 5000

Figure 47: Corrosion product morphology of samples exposed to pH 3.5 H_2SO_4 (Exposure time and magnification).

In H_2SO_4 solutions the corrosion product was seen a combination of two layers. A deeper layer was stuck to the material, followed by a top layer, non-attached. The top layer was removed if the samples were immediately cleaned after exposure.

In environments with pH 3.5 H_2SO_4 the main elements that form the product are C, O, Fe, Cr, N, Ca and S. A top layer of C and O is considered common on samples introduced from the laboratory environment caused by some contamination on the surface. Cr is part of the alloying elements and is expected to increase as it gets closer to the substrate surface. Ca and N come from atmospheric impurities, and S is superficially placed due to the corrosion accelerator used, H_2SO_4.

Based on the XPS results, a uniform composition of the corrosion product can be as follows. A superficial FeSO4 layer is placed on top of the layered corrosion prod-

uct. This is followed by compounds formed by a combination of Fe^{3+} and Fe^{2+} ions as part of metal oxides and hydroxides. FeOOH and Fe_2O_3 are closer to the surface while Fe2+ reduced species, Fe_3O_4 and FeO, are located near the substrate. As the corrosion proceeds the presence of Fe_3O_4 relative to Fe_2O_3 increases, but Fe_2O_3 is maintained dominant.

Samples exposed to pH 7 0.1 M initially exhibit a more granular morphology, which turns more flat with time. The layer looks like a closed structure, not permitting the easy access of corrosive species to the substrate. Initially the corrosion product is formed by a flowery structure γ-FeOOH and some β-FeOOH (akaganeite), Figure 48a. This last was not previously seen under H_2SO_4. Some shelling off of the film is observed, Figure 48b. By the 9th day some cotton balls are again visible, which could correspond to either β-FeOOH or α-FeOOH. In the 12th day black areas in the form of sphere-like globular formations are seen, that probably correspond to the spinel phase, Fe_3O_4 and/or Fe_2O_3, Figure 48c. γ-FeOOH stays dominant during the transformation until the 18th day, where different forms of β-FeOOH are found loose on top and in cigar shape, Figure 48. Crack are less visible than in H_2SO_4, due to the use of a less aggressive solution.

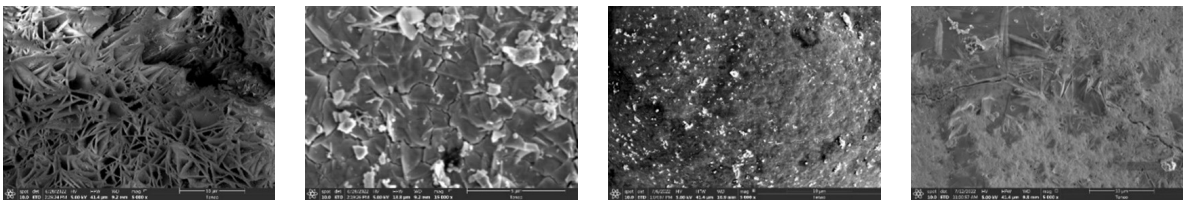

(a) 6th day x 5000 (b) 6th day x 15000 (c) 12th day x 5000 (d) 12th day x 15000

Figure 48: Corrosion product morphology of samples exposed to pH 7 NaCl 0.1 M (Exposure time and magnification).

The EDS mapping confirmed the presence of eight elements; Fe, O, C, S, P, Ca, Mn, Zn and Ti. The main elements are Fe and O, being Fe more present at zones where the corrosion product has not fully covered the substrate. By the 15th day the elements are more uniformly distributed showing no relevant accumulation, Figure 50. O increases with the newly formed oxides and the rest of the elements stay at smaller quantities. C and S show a slight increase with exposure time, probably due to the accumulation of contaminants.

In the XPS spectrums the main lines again correspond to C, O and Fe, with much less Na and Cr. The Na is due to the immersion in NaCl solution for corrosion acceleration, and Cr is from the alloying element of the steel, dissolved and incorporated into the rust in a uniform manner. Some argon (Ar) is also present, but this is due to the Ar+ ion sputtering. A top layer of C and O is again considered part of some

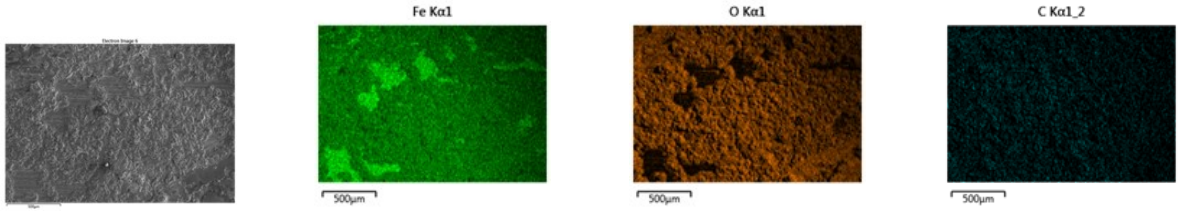

Figure 49: EDS mapping of the product, 9th day exposed to pH 7 NaCl 0.1 M.

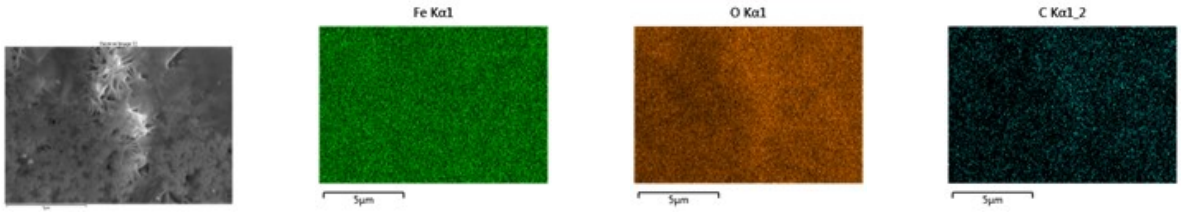

Figure 50: EDS mapping of the product, 15th day exposed to pH 7 NaCl 0.1 M.

contamination on the surface.

A common layer modelling is recognized, very similar to the one characterized in H_2SO_4 solutions. Fe^{3+} compounds with the highest degree of oxidation, FeOOH or Fe_2O_3 are again placed close to the surface. These are followed by a combination of Fe^{3+} and Fe^{2+} compounds, Fe_3O_4 and FeO closer to the substrate. The rust layer starts with a much higher presence of Fe^{2+} ions, while Fe^{3+} and OH^- increase with exposure time. The corrosion product on the surface exposed to pH 7 0.6 M was much more loose than in previous cases. This would easily fall apart and detach from the surface after drying. For this reason SEM micrographs were only taken after 9 and 15 days of exposure, due to contamination risks on the equipment. Equally, no XPS analysis could be performed. The product is mainly composed by γ-FeOOH flowery structures and α-FeOOH cotton balls, Table 12, Figure 51b. In the 15th day forms of β-FeOOH are found loose on top, Figure 51c, Figure 51.

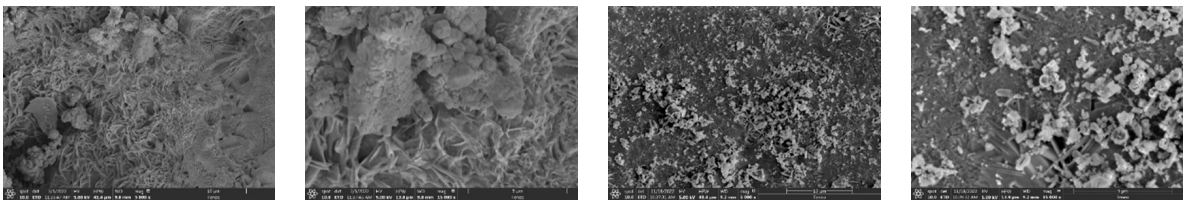

(a) 9th day x 5000 (b) 9th day x 15000 (c) 15th day x 15000 (d) 15th day x 15000

Figure 51: Corrosion product morphology of samples exposed to pH 7 NaCl 0.6 M (Exposure time and magnification).

Same elements were mapped under 0.1 M and 0.6 M, with O and Fe being the most present. Unlike in 0.1 M, zones with higher Fe from the substrate were already covered

by the 9th day, Figure 52. This suggests that the corrosion product developed more rapidly in the solution with higher molarity. This agrees with higher polishing needed in samples exposed to 0.6 M NaCl, as was illustrated in Figure 26. Different depths of the corrosion product are noticed due to a more irregular morphology. O was localized in some areas, and some aggregates were placed on top, containing C and S.

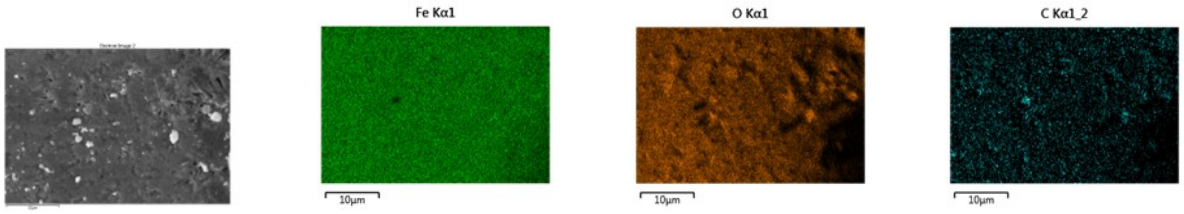

Figure 52: EDS mapping of the product, 9th day exposed to pH 7 NaCl 0.6 M.

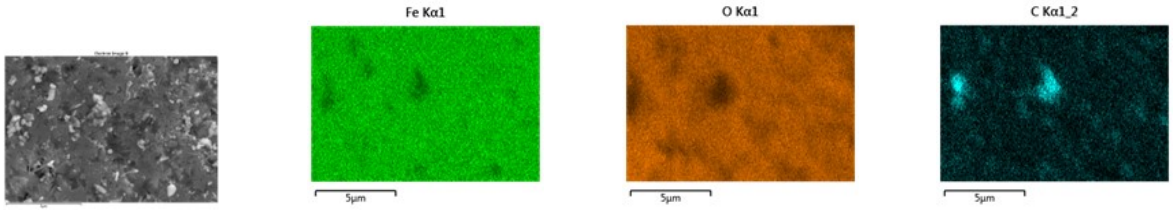

Figure 53: EDS mapping of the product, 15th day exposed to pH 7 NaCl 0.6 M.

4 Discussion

4.1 Quantification of absorbed hydrogen from the bearing steel

The bulk hydrogen in the non-corroded bearings was under the established 2 ppm limit, which was even more reduced with the polishing of the material. The significant variation in hydrogen was attributed to the presence of surface pits where corrosion product was accumulated. The material is not considered susceptible to contain bulk hydrogen as most of it corresponds to hydrogen stuck in the product. However, these can go deep in the material, making it susceptible to hydrogen damage in future applications. Moreover, pit clusters can be formed, Figure 39b, a sequestered group of pits that locate immediately adjacent to each other and can be more critical. A similar phenomenon was visible in bearings corroded in the pulp and paper industry, at which the hydrogen in the raceway was within acceptable hydrogen limits.

Pits are formed due to accelerated dissolution at localized sites such as inclusions and surface defects [22]. The growth of the localized corrosion can be characterized based on the change in chemistry associated with hydrolysis and electrolytic migration of the corrosive elements, forming a local aggressive environment [23]. The formation of local chemistry stabilizes the corrosion attack and forms a solution different to the exterior solution inside the pit. The morphology of the pits was found to differ between the non-corroded and service-exposed bearings. The pits in the non-corroded bearing were characterized by their superficially narrow but deep nature, while those in the service-exposed bearing were broader and shallow. The formation of deeper localized corrosion can be expected to cause a higher local acidification, which facilitates hydrogen evolution [24]. Authors such as Galvele [25] and Cerit et al. [26] observed that the hydrogen concentration inside the pit undergoes important changes when the pit size is changed, and that larger changes in composition and in pH are expected to be found at the bottom of the deeper pits. Consequently, the hydrogen that is absorbed in the material is enriched at the bottom of the pit.

Moreover, corrosion induced pits can act as stress concentrators from which cracks could form by intensify the local stress field, and reducing the components load carrying capacity [26]. Firstly, the pitting-corrosion induced roughness on the surface can lead to local stress concentrations, and the concentration of local stresses at pits can induce stress induced hydrogen diffusion into the material [24]. Hiroses et al. [27] observed that crack branching originating from a pit were related to dislocation-hydrogen interactions.

Therefore, pits can be used as hydrogen traps, affecting hydrogen distribution in the material, and leading to localized hydrogen enrichment. This would lead to inhomogeneous distribution of hydrogen throughout the material, different to what would be expected considering only the hydrogen product during the formation of the top uniform corrosion layer. The criticality of these pits in the present work is hard to define due to variations of the cross-sectional shape, and the uncertainty of the environmental conditions at which these were applied. The morphology and growth of the pit is defined by the environmental parameters and the microstructure of the steel, which lead to a defined corrosion attack and a specific pitting mechanism. This will influence the continuation of the corrosion process and the hydrogen absorption in future applications. This highlights the insufficiency of visual inspection alone in detecting the presence of small pits, and determining the needed remanufacturing procedure.

4.2 Hydrogen accumulation in the material and polishing process

It is initially hypothesized that increasing the amount of polished material would noticeably decrease hydrogen concentration due to its accumulation in the first atomic layers. However, no clear relationship could be established between polished material and hydrogen in the bulk. The complexity of the phenomenon is attributed to the multitude of parameters that are involved, as bearing steels are known to contain many types of inclusions, impurities and inhomogeneities which affect hydrogen movement through the material [6]. The hydrogen transport and placement in the metal is defined by two main phenomena: physicochemical reactions with microstructural characteristics of the material and the physical diffusion of hydrogen through the concentration gradient [6]. Moreover, the quantification of hydrogen and its distribution across the various trapping sites is a challenge, as the nature of the traps defines if these are reversible, irreversible, saturable, not saturable, and so on, defining the hydrogen movement and location.

Inclusions such as TiC particles have been studied by several authors [28] due to their strong attractive interaction energy with hydrogen. Moreover, discontinuities such as voids showed a preferred location at grain boundaries and the interface between the steel matrix and chromium carbides [29]. The composition of the bearings analyzed was slightly different, Table 1 and Table 2, with Bearing A containing 0.96% C and Bearing B containing 2.91% C. It was observed that the diffusivity of hydrogen tend to decrease as steel grade increases with the carbon content [6]. Hadam and Zakroczymski [11] saw that the lattice hydrogen diffusivity in a low-carbon steel was higher, and the

subsurface thickness where hydrogen was stored was 25 times higher than in a high-carbon steel. The distribution is influenced by the higher amount of potential hydrogen traps in the high-carbon steel, which requires less material to be polished for the removal of the subsurface hydrogen.

The hydrogen is expected to be unevenly distributed throughout the cross section of the specimens due to accumulation of traps at the subsurface. The challenge is intensified when the metal is subject to stresses [11] . The bearing contact cycle and the formed residual stresses condition the hydrogen diffusion into the material through stress-assisted diffusion. A maximum Von Mises stress and corresponding plastic strains appear at the subsurface. The strain gradient will result in a corresponding gradient of hydrogen trap density and thus a gradient of trapped hydrogen content [28].

While acknowledging that the amount of polished material may have relevance in the amount of hydrogen in the bulk, the studied cases cannot be directly compared due to their exposure to different environments and the lack of equivalency in their levels of the formed corrosion. The overcoming of the 2 ppm in the higher carbon steel is attributed to the extreme conditions from the chamber, as this could not be linked to the hydrogen distribution. Both materials should be exposed to same environmental conditions for significant conclusions.

4.3 The effect of polishing and the newly generated surface on the presence of hydrogen

The effect of sample preparation methods on the hydrogen determination at ppm levels often need to be considered, as the surface removal and the sample cleaning method may cause hydrogen to diffuse out or into the material. Mahbo et al. [1] observed higher hydrogen concentration in samples scraped with SiC paper to remove a zinc coating from steel. The paper could contaminate the surface making it more rough and susceptible to water adsorption, carbides, and other contaminants, leading to a higher presence of hydrogen. The process could also entail the formation of elements such as surface defects, internal stresses, and plastic deformations [30].

The coatings in metals could be expected to act as a barrier film for hydrogen entry by changing the hydrogen evolution kinetics at the surface and cause a delay by interfering with the hydrogen absorption [31]. However, the pre-polished material was seen to be less susceptible to hydrogen absorption, with more consistent results and much less scatter. It is known that corrosion rate increases with an increase in sur-

face roughness [30], while a smooth surface reduces the presence of micro-reaction sites which trap corrosion product and promote growth of pits. The higher hydrogen concentration in non-polished material could indicate that hydrogen is distributed in the coating in locations such as the pits visible in Figure 39b, and that polishing reduces the number of sites that could activate a metastable pit growth. The elimination of the hydrogen accumulation sites also lead to less scatter, and more consistent results.

Moreover, studies such as the one followed by Charca et al. [32] observed that surface imperfections or defects would affect the behavior of hydrogen in a given material. These could cause diffusion through short circuit paths causing enhancement of diffusion rates of hydrogen atoms. The removal of the coating generates a more homogeneous and defect-free surface, achieving a more uniform surface for hydrogen to react with, leading to more consistent results. A smooth surface is also expected to be less susceptible to contaminant absorption due to a lower surface area.

4.4 Mobility and trapping of absorbed hydrogen in the steel

The thermal desorption spectroscopy (TDS) technique was used to study hydrogen-trap interactions. The nature of a trap in a material can be reversible or irreversible based on the activation energy needed for the hydrogen atom to leave the site. Reversible traps are usually interstitial sites that require low activation energy, while in irreversible traps a higher activation energy is required for hydrogen to leave the site. The total bulk hydrogen is analyzed in the study of hydrogen in MET while part of the hydrogen is only detected in the TDS, released at temperatures covered by the applied method. The desorption peaks correspond to hydrogen stored at reversible traps, which typically diffuse throughout the material, or is desorbed at temperatures below 400 °C [33]. The hydrogen at deeper traps needs higher activation energy and is not visible in the spectrums.

The reversibly trapped or diffusible hydrogen is considered to dominate the hydrogen enhanced damages. In the present work the trapped fraction of hydrogen was seen to be the most present, reducing the risk of hydrogen damage even at conditions at which high hydrogen saturations were detected. The hydrogen mobility within the material is seen to be very low. Hydrogen is more deeply trapped in the track of the inner ring in contact with the rollers and in the part in contact with the shaft. The hydrogen accumulation at deeper traps may be caused due to deformations during the service life, where continuous contact with the rollers and the repeated loading and unloading cycles cause microplasticity. The subsurface zone can be plastically deformed, and the crystal structure distorted, forming vacancies and new trapping sites where hydrogen

atoms can be placed [5]. Hydrogen can then be irreversibly trapped in microstructural defects such as dislocations, vacancies, and grain boundaries, with higher binding energies. This is expected to be unevenly distributed throughout the sample thickness, with most of the trapped hydrogen stored in the subsurface region [2]. The trap site density is considered a key factor in the amount of hydrogen absorbed.

At room temperature hydrogen diffusion throughout the material or coming out of the steel happens. The outdoor time before MET and TDA allows most diffusible hydrogen to escape from the sample, primarily revealing the reversibly trapped hydrogen. The effusion of diffusible hydrogen starts immediately after samples are taken out of the chamber due to the high hydrogen mobility in the material. Duprez et al. [4] studied the impact of mobile hydrogen in high-strength steels, and a significant ductility loss was observed during immediate mechanical tensile testing after hydrogen charging. The ductility properties were recovered once hydrogen was diffused out of the material indicating that did not cause hydrogen-enhanced damage. This could indicate the recoverability of the mechanical properties with hydrogen desorption from the metal.

The diffusible hydrogen is expected to be desorbed at different rates throughout the exposure. In the early stage of desorption, hydrogen is released relatively faster than that in the subsequent stage [11]. Part of the hydrogen that is first diffused correspond to hydrogen adsorbed on the outer surface of the steel. This is followed by hydrogen stored at the subsurface region where more trapping sites are found and are more saturated than other sites deeper in the metal. Nonetheless, the rate of hydrogen is also influenced by the nature of the corrosive media, and the formed product. This was studied by various authors [11], [34] who addressed that the formation of the corrosion product not only influences the hydrogen generation through surface chemical reactions, but also the following hydrogen desorption process. The formed product can avoid the hydrogen desorption out of the material and cause retardation of desorption peak at low temperatures [2] by not allowing the mobile hydrogen to leave the sites. The desorption becomes more difficult, influenced by the hydrogen mobility throughout the formed corrosion product defined by the density and stability of the layer. Therefore, the effusion happens more easily once the bearing is remanufactured. This means that the risk of the mobile hydrogen in the material is still present during the continuous application of the bearing.

Additionally, during the 24 h of exposure, hydrogen also diffuses to other features at which hydrogen is stored at different binding energies. The diffusion of hydrogen to these features cause changes in the hydrogen distribution, leading to a shift in the

desorption peak. Sites with a more reversible character often act as hydrogen sources, as hydrogen can still be mobile through the material. Reversibly trapped hydrogen can then move to sites with higher binding energies, resulting in higher peak temperatures as in Figure 37. The ability of hydrogen to diffuse to different features is an important factor, as this is often an indicator of the possibility of hydrogen-enhanced damage [1]. The hydrogen sources in the material can donate the hydrogen to features that can be critical for the failure of the material.

4.5 Formed corrosion product and hydrogen absorption

Corrosion product formation and morphology varied with the corrosive environment, and dynamic conversions between different products were observed. Literature relates specific morphologies to particular compounds.

The different applied corrosive media influenced the hydrogen behavior in bulk. An explanation for this is that once the corrosion product covers the steel surface the hydrogen adsorption can become negligible due to the low diffusivity through the formed oxides [3]. Then, the changes in the solution pH control the hydrogen entry into the steel. The hydrogen permeation is then affected by pollutants found in the environment. Further corrosion can be expected at a higher concentration of SO_2 and Cl^-, which is becoming more harmful for the steel [35]. However, the corrosion rate of the metal is generally not constant. There is an initial increase in corrosion rate followed by a decrease with exposure time due to the accumulation of rust layers on the surface, which enhance corrosion resistance. Morcillo et al. [35] observed that the corrosivity of SO_4^{2-} and Cl^- anions had a similar tendency in carbon steels. At low concentrations, the corrosion rate was very low. It would increase by increasing the concentration until a point at which further increase in concentrations did not increase the corrosion rate. Instead, it reached a steady state.

The initial corrosion of the iron comes with the following process, where first, the anodic dissolution reaction happens as [9],

$$Fe \rightarrow Fe^{2+} + 2e^- \tag{8}$$

$$Fe^{2+} \rightarrow Fe^{3+} + e^- \tag{9}$$

Followed by the corresponding cathodic reaction in an acidic environment,

$$2H^+ + 2e^- \rightarrow H_2 \tag{10}$$

$$O_2 + 4H^+ + 4e^- \rightarrow 2H_2O \tag{11}$$

$$2H_3O^+ + 2e^- \rightarrow H_2 \uparrow + 2H_20 \tag{12}$$

The Fe^{2+} convert to $FeOH^+$ and $Fe(OH)_2$ by hydrolysis,

$$Fe^{2+} + H_2O \rightarrow FeOH^+ + H^+ \tag{13}$$

$$Fe^{2+} + 2H_2O \rightarrow Fe(OH)_2 + 2H^+ \tag{14}$$

by extending exposure time the $Fe(OH)_2$ and $FeOH^+$ further oxidize to FeOOH as,

$$Fe(OH)_2 \rightarrow FeOOH + H^+ + e^- \tag{15}$$

$$2FeOH^+ + 1/2O_2 + H_2O \rightarrow 2FeOOH + 2H^+ \tag{16}$$

$$2Fe(OH)_2 + 1/2O_2 \rightarrow 2FeOOH + H_2O \tag{17}$$

At other points, the two electrons will be used up in cathodic reduction to Fe_3O_4

$$Fe^{2+} + 8FeOOH + 2e^- \rightarrow 3Fe_3O_4 + 4H_2O \tag{18}$$

and Fe^{3+} ferrous ions hydrolyze to FeOOH and Fe_2O_3 as,

$$Fe^{3+} + 2H_2O \rightarrow FeOOH + 3H^+ \tag{19}$$

$$2Fe(OH)_3 \rightarrow Fe_2O_3 + 3H_2O \tag{20}$$

Hydrogen is therefore produced in the cathodic reaction and the hydrolysis reaction. The corrosion product in all cases consisted of ferric oxyhydroxides and oxides. However, the process is continued based on the applied solution, and certain compounds are formed from the influence of the corrosive agents.

4.5.1 Corrosion under H_2SO_4 corrosive environments

The XPS results confirmed a layered structure in samples exposed to H_2SO_4. The corrosion product was formed by FeO in contact with the base metal, followed by Fe_3O_4 and Fe_2O_3 in varying quantities, and top FeOOH compounds. Fe^{3+} and Fe^{2+} ions are part of metal oxides and hydroxides. These are mainly Fe_2O_3 and lower amounts of Fe_3O_4. Fe^{3+} and Fe^{2+} ions increase with deepness and exposure, with a relatively higher amount of Fe^{3+}. Fe_2O_3 is formed on top, which combines with increasing contents of Fe_3O_4 as it gets more profound, and has the lowest FeO layer. A superficial $FeSO_4$ layer is also confirmed, whose presence initially increases and decreases. Fe oxidizes with the formation of ferrous sulfate $FeSO_4$ and H_2 as [9],

$$Fe^{2+} + SO_4^{2-} \rightarrow FeSO_4 \tag{21}$$

$$2Fe(OH)_2 + SO_4^{2-} + 2H^+ \rightarrow FeSO_4 + 2H_2O \tag{22}$$

No hydrogen ions are produced throughout the formation of $FeSO_4$. However, $FeSO_4$ can be further oxidized to become FeOOH with the formation of H^+ ions as follows [36].

$$FeSO_4 + 2H_2O \rightarrow FeOOH + SO_4^{2-} + 3H^+ \tag{23}$$

Many forms of FeOOH were found as part of the corrosion product in environments containing SO_4^{2-} , independent of the pH. In both cases, flowery structures grow irregularly from a more even surface with crater-like shapes. The flowery structure corresponds to γ-FeOOH, transforming into α-FeOOH cotton ball structures. The product is spread in a more uniform way covering the surface. γ-FeOOH seems to cover most of the surface by the end of the test.

It could be that SO_4^{2-} ions produced in Equation 23 are repeatedly used to form $FeSO_4$ from Equation 21 and Equation 22 [36]. Products from the H_2SO_4 solution could also be expected to contain iron sulphide (FeS) [37], but these were not recognized in the present work.

The compactness of corrosion products strongly depends on the concentration of H_2SO_4 [37] and the corrosion rate on the degrees of densification and crystal structures of the iron sulphide compounds formed [38]. Under pH 3.5, fewer cracks were visible, suggesting a lower aggressiveness of the applied solution, which could prevent the entrance of corrosive agents from getting in contact with the metal, avoiding further corrosion.

In material exposed to H_2SO_4 an initial increase of hydrogen content is observed, followed by a decrease on day 9 for pH 3.5 and day 6 for pH 1.5. The initial increase in absorbed hydrogen is possibly due to the generation of H^+ ions during the production of initial products such as $Fe(OH)_2$, $FeOH^+$ and FeOOH. Moreover, the product must still be thick/dense enough to avoid hydrogen entrance. The later formation of Fe_2O_3 and Fe_3O_4 is not accompanied by hydrogen generation, as these are produced by reducing the FeOOH. The lowering of the hydrogen could also be related to the protective $FeSO_4$ layer [39], whose formation is not accompanied by hydrogen liberation, but rather H^+ ions may be consumed [9]. Additionally, the surface now covered by the corrosion product would also retard the hydrogen reduction reaction and the transport of the corrosive media to the substrate.

In both cases, the lowering of absorbed hydrogen is followed by a final increase, Figure 22 and Figure 23 . This can occur due to continuous exposure to atmospheric humidity in the chamber. If the acid absorbs the water vapor from the humid atmosphere this can become even more corrosive [40]. The absorption can also occur through the $FeSO_4$ layer previously formed, which undergoes hydration, or by acid entrapped. If the acid retained by the sulfate layer reacts with the steel after dilution, this may induce even higher corrosion rates [39]. Also, the possibility of SO_4^{2-} ions forming during the oxidation of $FeSO_4$ (Equation 23), serving as autocatalysis, can lead to an increase and accumulation of SO_4^{2-} ions with exposure time. As a result, a continuous acceleration of corrosion reaction can happen [36]. Moreover, at some point, the $FeSO_4$ film can become unstable due to the oxidation of Fe^{2+} ions to Fe^{3+} ions. Banks and Sudbury [41] observed that the oxidation causes the film to be more porous and, therefore, less protective.

4.5.2 Corrosion under NaCl corrosive environments

NaCl solutions with different concentrations simulated two atmospheres with different chloride deposition rates. In atmospheric environments, NaCl dissolves into water and decomposes into a mixture of cation (Na^+) and anion (Cl^-). Cl^- is the most corrosive ion with a higher tendency to catch electrons from the metal surface. Therefore, the corrosion rate mainly depends on Cl^-, while the effect of Na^+ might be negligible [35]. In carbon steels, the formed corrosion is generally uniform. However, the presence of Cl^- could cause some pitting at the surface [42]. This was noticeable during the polishing of samples exposed to NaCl, where part of the removed material was done due to localized corrosion products in formed pits—the susceptibility of the steel to pitting corrosion increases with increasing NaCl concentration [43].

The corrosion product is notably more dense, thick, and irregular than in H_2SO_4. The formation of a thicker corrosion product could be linked to a higher Cl concentration (0.6 M NaCl), as was previously addressed by studies such as the one followed by Wang et al. [44]. The solution containing fewer Cl^- ions show a higher lack of continuity (0.1 M NaCl) and become thicker and more continuous in the more concentrated saline solution. However, the formed product also becomes more fragile and with great porosity, containing some voids and intralayer rust bands. This lead to the detachment of layer fragments, as part of the corrosion product exhibits poor adhesion to the substrate. The detachment of the product could result in the substrate becoming exposed, without any additional protection, thereby accelerating the corrosion process upon re exposure to the environment [45]. However, during application the robustness of the product could avoid hydrogen absorption maintaining the low amount of hydrogen in the bulk through exposure, as seen in Figure 25.

Under NaCl a multilayered corrosion product can be expected to be structured as alternate compact layers and loose interlayers. The main layers contain Fe_3O_4 (magnetite) and/or γ-Fe_2O_3 (maghemite), and β-FeOOH (akaganeite). In-between Fe_3O_4 and γ-Fe_2O_3 non-stoichiometric compounds with a general formula $Fe_{3-x}O_4$ are present, where x varies from 0 to 1/3 [46]. γ-FeOOH (lepidocrocite) and α-FeOOH (goethite) are also present in varying proportions through the layers [45]. These are the main products forming the outermost layer that covers the multi-layered product, with some β-FeOOH in smaller proportions. The product is superficially primarily comprised of a flowery structure of γ-FeOOH, which turn into cotton-like structures upon exposure, α-FeOOH. The dominance of γ-FeOOH is maintained throughout the corrosion process. This is usual in all carbon steels [45] as observed in the environment containing H_2SO_4. Unlike in environments containing SO_4^{2-}, β-FeOOH is only formed in the presence of Cl^- ions.

In all environments, γ-FeOOH and α-FeOOH were detected. These two compounds are typically found in the corrosion products formed on carbon steels exposed to atmospheric corrosion. However, these are porous in nature, and the product layers' adhesion to the substrate is as well. The porousness and limited adhesion to the substrate were reported by Xiao et al. [47]. As a result, the corrosive species can penetrate the corrosion layers and reach the metal surface. Fe_3O_4 and γ-Fe_2O_3 are more active than a protective role in the corrosion process [48].

The chemical dynamics can be as follows. The chloride concentration in the aqueous layer gives rise to the formation of ferrous chloride which hydrolyses the water, causing

an increase in the acidity of the electrolyte and accelerating the corrosion process [45].

$$FeCl_2 + H_2O \rightarrow FeO + 2HCl \tag{24}$$

During surface wetting, γ-FeOOH is first reduced into a transition phase of γ-Fe.OH.OH in the cathodic process, which can balance the anodic dissolution of Fe [49]. Until the FeOOH has been used up, the cathodic process is dominated by the O_2 reduction. Then, γ-Fe.OH.OH is oxidized into γ-FeOOH again.

$$\gamma - FeOOH + H^+ \rightarrow \gamma - Fe.OH.OH \tag{25}$$

$$1/2O_2 + H_2O \rightarrow 2OH^- \tag{26}$$

$$2\gamma - Fe.OH.OH + 1/2O_2 \rightarrow 2\gamma - FeOOH + H_2O \tag{27}$$

During the stabilization of the product, part of γ-FeOOH can dissolve into amorphous ferric oxyhydroxide, which would turn into α-FeOOH by solid-state transformation. On the other hand, a majority of ferric rust can be o reduced to Fe_3O_4. The change of γ-FeOOH to Fe_3O_4 is as follows,

$$2\gamma - FeOOH + Fe^{2+} \rightarrow Fe_3O_4 + 2H^+ \tag{28}$$

Moreover, the low contents of β-FeOOH indicate that most of it has already been consumed and reduced to Fe_3O_4, as,

$$2\beta - FeOOH + Fe^{2+} \rightarrow Fe_3O_4 + 2H^+ \tag{29}$$

In environments containing high amount of Cl^-, another possible forming process of γ-FeOOH is as follows [47],

$$(Fe^{2+}, Fe^{3+}) + Cl + OH \rightarrow FeOCl \tag{30}$$

Under dry conditions,

$$FeOCl \rightarrow \gamma - FeOOH \tag{31}$$

The main spinel phase formed under NaCl on carbon steels is considered Fe_3O_4 independent of immersion time and concentration in the solutions [48].

The molar concentration affected hydrogen absorption, as more hydrogen was found under 0.1 M compared to the 0.6 M solution. A lower concentration could be considered less corrosive and could more hardly overcome the oxide film previously formed [35] or [42]. However, some studies, such as the one followed by Marqui et al. [50], address a lower oxygen solubility in the solution layer, a fundamental element for the cathodic process, which could lead to less corrosion. For high chloride concentrations, the adsorbed oxygen concentration on the metal surface is lower in contrast to the adsorption of chloride ions. This is because there is a continuous decrease of oxygen solubility related to an increase in NaCl concentration above a certain concentration.

Initially, the corrosion process is believed to be led by the transportation of oxygen to the corroded surface. As the product grows, oxygen diffusion is impeded, and the process becomes dependent on the degree of porosity and the packing of the rust constituents [48]. The poor presence of oxygen favors the formation of Fe_3O_4, and a gradient is formed through the product with the smallest value at the metal surface, where Fe^{2+} oxidizes to Fe^{3+} , forming the Fe_3O_4 [48].

Continued corrosion of iron can also lead to the formation of $Fe(OH)_2$. At low temperatures, this is known to be stable but converts to Fe_3O_4. This transformation might be significant when studying the amount of absorbed hydrogen as additional hydrogen is produced if $Fe(OH)_2$ converts to Fe_3O_4 [43]. As Reardon proposed, the corrosion of iron occurs by the following oxidation reaction in a neutral, alkaline environment;

$$Fe(s) + 2H_2O(l) \rightarrow Fe^{2+} + 2OH^- + H_2(g) \tag{32}$$

And $Fe(OH)_2$ converts to Fe_3O_4 as;

$$3Fe(OH)_2(s) \rightarrow Fe_3O_4(s) + H_2(g) + 2H_2O(l) \tag{33}$$

Additional H_2 is generated for every mole of iron corroded if all of the produced Fe $(OH)_2$ is transformed. This could support the increased absorption by the exposure's end under NaCl solutions. Moreover, the relative abundance of Fe_3O_4 does not stay constant in time but exhibits oscillations that increase with NaCl concentrations. Pereze et al. [48] could conclude that there is no evolution of Fe_3O_4 towards a protective behavior with exposure time. The abundance of Fe_3O_4 leads to a non-protective/active layer.

Certain elements found in XPS could also affect the formation of the corrosion product. C stabilizes magnetite against oxidation, Cu produces pure Fe_3O_4 by inhibiting

the formation of α-FeOOH, and that Cr promotes the formation of α-FeOOH [51].

It is important to consider the small hydrogen content analyzed in the present study. Even in extreme conditions the maximum exposure time, up to 18 days, is very limited, as corrosion tests often take up to years to obtain relatable results. Small hydrogen contents lead to considerable scatter. However, some other studies with much higher hydrogen charging addressed a continuous increase of hydrogen with exposure time. Mabho et al. [1] confirmed that longer exposure time in samples charged through an electrolyte solution resulted in more hydrogen absorption. They observed this trend in both H_2SO_4 and NaCl solutions.

Some studies [48] also tried to understand the effect of different steel compositions containing variable alloying elements. They analyzed ranges of C, Si, Mn, S, P, Ni, Cr, Al, Cu and Sb under aqueous medium containing Cl^-. They observed that the corrosion product buildup's variable behavior only lies in the high presence of Si, P, Ni and Cr. The presence of elements could mainly change the number and type of reaction sites, favoring nucleation of the corrosion [52]. However, these were present in very small quantities, and no specific influence can be considered.

5 Conclusions and recommendations

The main objectives of this study were to explore insights into the corrosion and hydrogen absorption of the remanufactured bearing steel. The following conclusions are highlighted by the intensive analysis.

The first research gap was focused on how the environmental conditions could determine the corrosive behaviour of the steel. The following conclusions were obtained.

- The hydrogen absorption is enhanced by certain corrosive environments that raise chemical reactions, and more hydrogen is produced. The rate of hydrogen uptake is influenced by the type of solution applied, the exposure time and the resulting corrosion products formed.
- Absorbed hydrogen is not an increasing function of exposure to the corroding media, but a combination factor such as the coverage of the surface by the product, and the reduction and consumption of hydrogen by the surface chemical reactions. The absorption is also determined by the density and compactness of the product formed.
- Pits are found, formed due to accelerated dissolution at localized sites. Their morphology and growth are influenced by environmental parameters and the microstructure of the steel, and the formation of deeper localized corrosion can be expected to facilitate hydrogen evolution at localized sites, leading to hydrogen accumulation.

The second research gap to be addressed was whether the remanufacturing process involving polishing can guarantee the required operational performance of corroded bearings for future applications.

- The remanufacturing process by polishing did ensure the needed operating capabilities of the corroded bearing from pulp and paper industry by assessing the hydrogen content under the stablished acceptable limit of 2 ppm. In more extreme conditions the boundary could not be ensured, and the danger of hydrogen enhance damage is still present. An standard amount of removed material cannot be determined, and should be adjusted to specific corrosive environments.
- The hypothesis that increasing the amount of polished material would decrease hydrogen concentration could not be supported. This is due to the complexity of the hydrogen behavior in bearing steels influenced by inclusions, impurities, and inhomogeneities in the material. The transport and placement of hydrogen in the metal are influenced by both physicochemical reactions and physical diffusion.

- Fluctuations in bulk hydrogen can be attributed to the presence of pits. Pits can be used as hydrogen traps and affect hydrogen distribution in the material, leading to localized hydrogen enrichment. The visual inspection alone seems to be insufficient in detecting the presence of small pits and determining the needed remanufacturing procedure.

- It is concluded that part of the hydrogen is distributed in the coating in locations such as visible pits, and polishing reduces the number of sites that could activate a metastable pit growth. The elimination of surface hydrogen accumulation sites and imperfections leads to a more uniform surface for hydrogen to react with, leading to more consistent hydrogen absorption. A smooth surface is also less susceptible to contaminant absorption due to a lower surface area.

- The machining parameters and polishing process followed by the remanufacturing company could not be addressed. The reliability and comparability of the followed polishing and inspection process are questionable to present solid statements. The manual polishing and the single point measurements do not cover the irregularities in the corrosion product. The influence of sample preparation might also have caused the hydrogen to diffuse out or into the sample.

Research gap 3 was focused on the understanding of how exposure to various conditions affects the diffusion and accumulation behaviour of hydrogen in bearings. It could be concluded that;

- Hydrogen is transported by diffusion and localization into the internal sites of the metal. The corrosive environment defines the generation and absorption of hydrogen, and the nature and trapping behavior. The complexity resides in the variable trapping sites found in the analyzed steel.

- The trapped hydrogen was seen to be dominant reducing the risk of hydrogen damage even at high hydrogen saturations. The risk for hydrogen induced damage can be qualified as low considering this is dominated by reversibly trapped hydrogen.

- The dominancy of deeply trapped hydrogen can be due to microplasticity, and trapping sites formed during service life, as different zones in the bearing exposed different hydrogen trapping behaviour.

- Hydrogen diffusion out of the material occurs after exposure, and most reversible hydrogen escapes from the material. This could entail the recoverability of mechanical properties lost while the hydrogen was placed in the bulk. The rate of hydrogen desorption is influenced by the nature of the corrosive media, exposure

time and the formed product. The effusion happens more easily once the bearing is polished, meaning that the risk of the mobile hydrogen in the material is still present during the continuous application of the bearing.

- The redistribution of hydrogen to other features is observed. This showed that reversible traps can act as hydrogen sources in the material donating hydrogen to features that can be critical for the failure of the material. This is an indicator of the possibility of hydrogen-enhanced damage.

Based on the findings and conclusions of the research, several recommendations are proposed for coming works. These recommendations are aimed to improve the understanding of hydrogen damage mechanisms and improve the effectiveness of the proposed remanufacturing process.

- A more comprehensive investigation into the impact of different environments and chemical agents needs to be conducted. The variability of chemicals in the pulp and paper industry can be considered a risk for the operation of the bearing component, leading to high contents of bulk hydrogen. The remanufacturing process can then be adapted to the requirements of each environment.

- The effect of the material composition and the alloying elements can be significant, and therefore should be more thoroughly considered. Inclusions present in bearing steels are important in the understanding of hydrogen trapping behaviour, as these are expected to have an influence on the localized corrosion, build-up of the product, and the hydrogen trapping at these locations.

- The presence of localized corrosion should be further studied, as these could act as hydrogen accumulation sites and nucleation sites for hydrogen induced damages. Furthermore, relying solely on visual inspection to determine the absence of corrosion products in the bearing may not be sufficient. The use of more advanced technical equipment capable of detecting the presence of such traps would be needed.

- TDS tests under same conditions should be repeated at different heating rates to determine the activation energy of the traps found. Though the variation of the method and the heating rate applied the trap activation energy can be determined from the change in the peak temperature. Then each activation energy can be linked to a specific trapping site, and the risk of the hydrogen can be better understood.

- A more detailed inspection of the received spectrums should be followed. Gaussian peaks that overlap in the spectrum need to be fitted in the obtained spectra

to obtain more accurate information about how hydrogen is trapped. Various simulation models are proposed in literature for this purpose.

6 Appendix

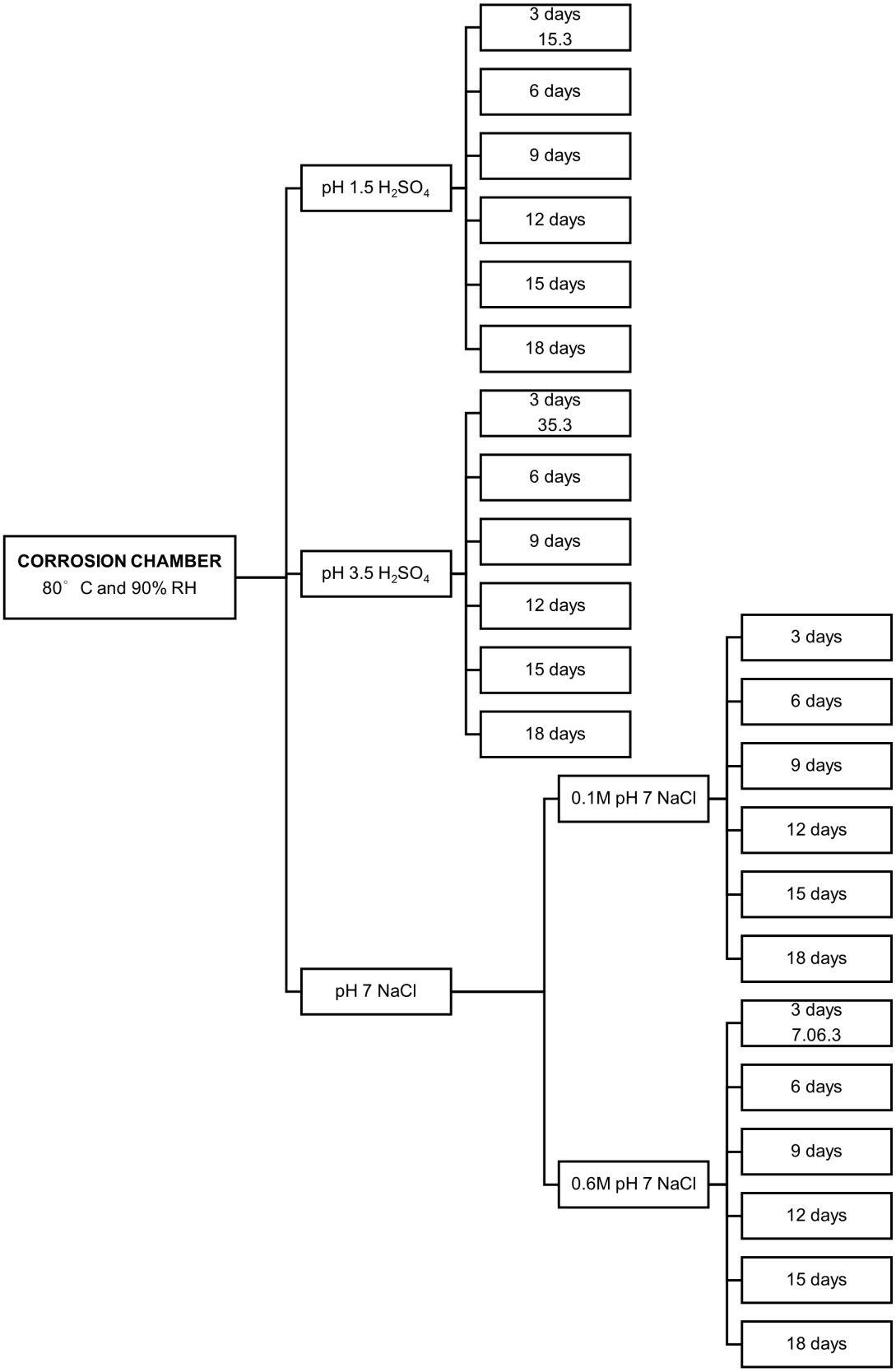

Figure 54: *Overview of samples placed in the corrosion chamber. These are organized based on the applied corrosive media and the exposure time.*

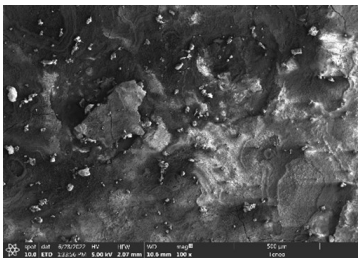

(a) x100

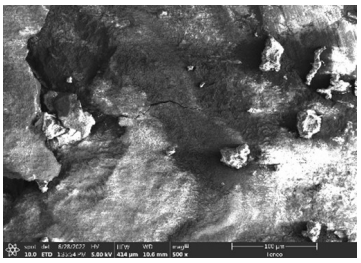

(b) x500

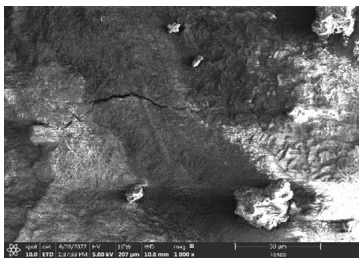

(c) x1000

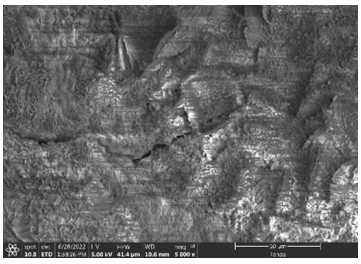

(d) x5000

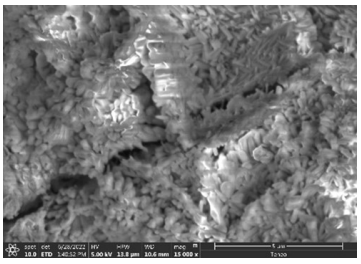

(e) x15000

Figure 55: Corrosion product on samples exposed to pH 1.5 H_2SO_4 9 days

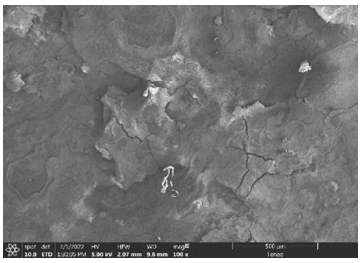

(a) x100

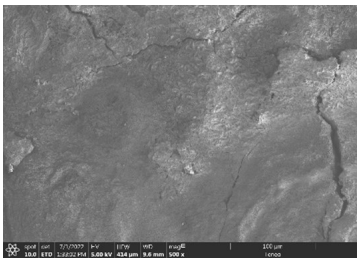

(b) x500

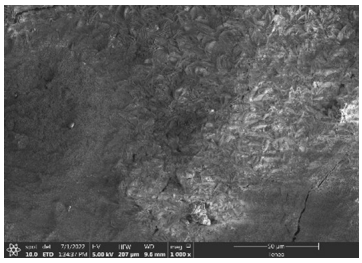

(c) x1000

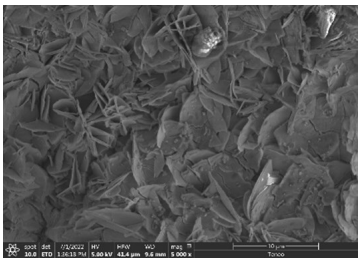

(d) x5000

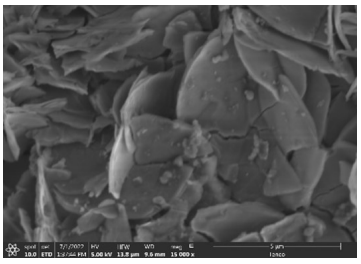

(e) x15000

Figure 56: Corrosion product on samples exposed to pH 1.5 H_2SO_4 12 days

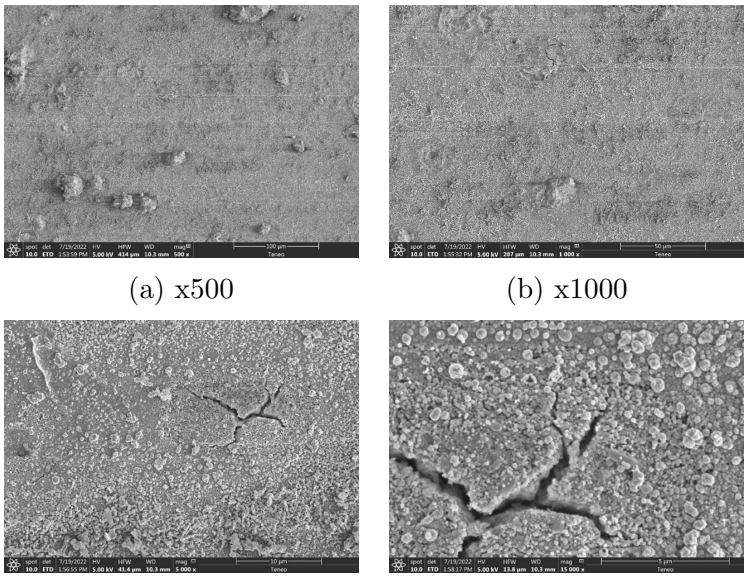

(a) x500 (b) x1000

(c) x5000 (d) x15000

Figure 57: Corrosion product on samples exposed to pH 1.5 H_2SO_4 15 days

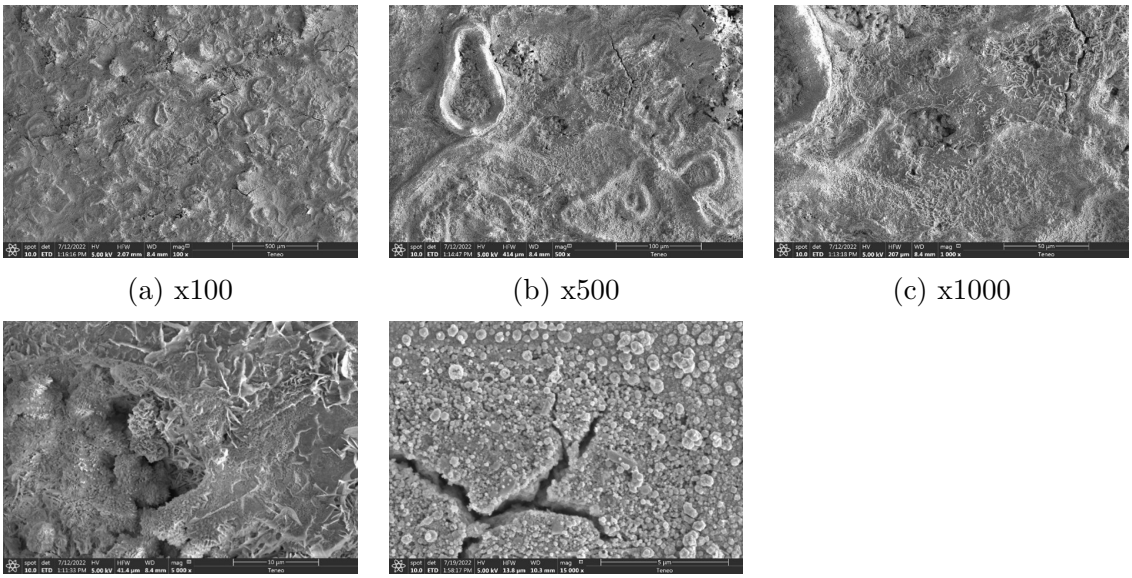

(a) x100 (b) x500 (c) x1000

(d) x5000 (e) x15000

Figure 58: Corrosion product on samples exposed to pH 1.5 H_2SO_4 18 days

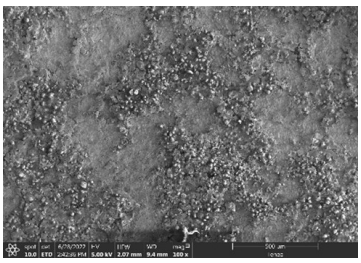

(a) x100

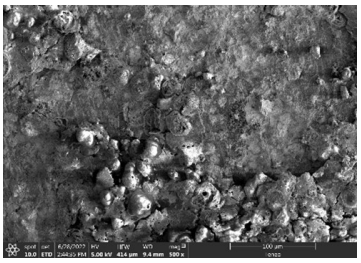

(b) x500

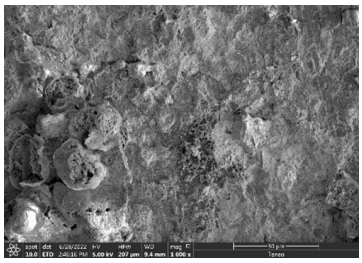

(c) x1000

(d) x5000

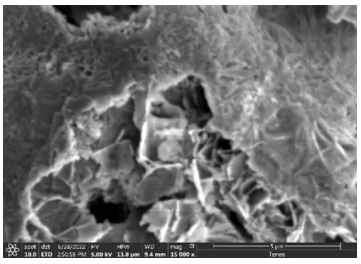

(e) x15000

Figure 59: Corrosion product on samples exposed to pH 3.5 H_2SO_4 9 days

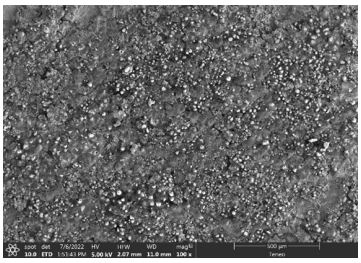

(a) x100

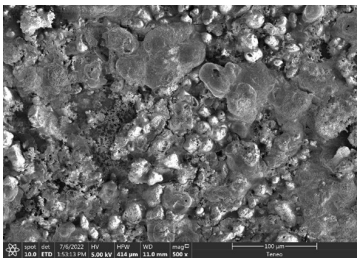

(b) x500

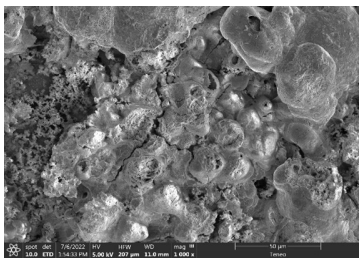

(c) x1000

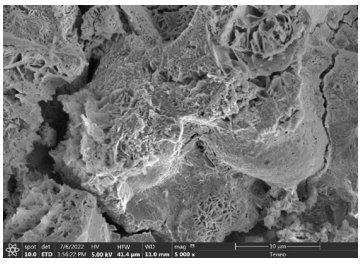

(d) x5000

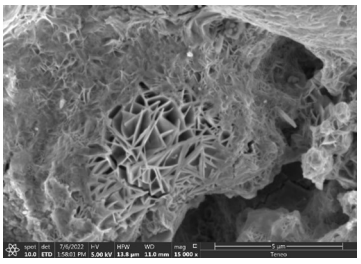

(e) x15000

Figure 60: Corrosion product on samples exposed to pH 3.5 H_2SO_4 12 days

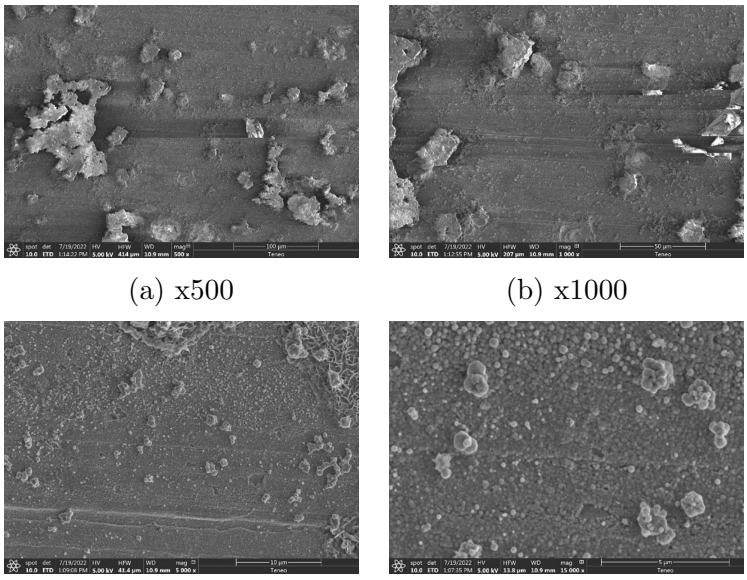

(a) x500 (b) x1000

(c) x5000 (d) x15000

Figure 61: Corrosion product on samples exposed to pH 3.5 H_2SO_4 15 days

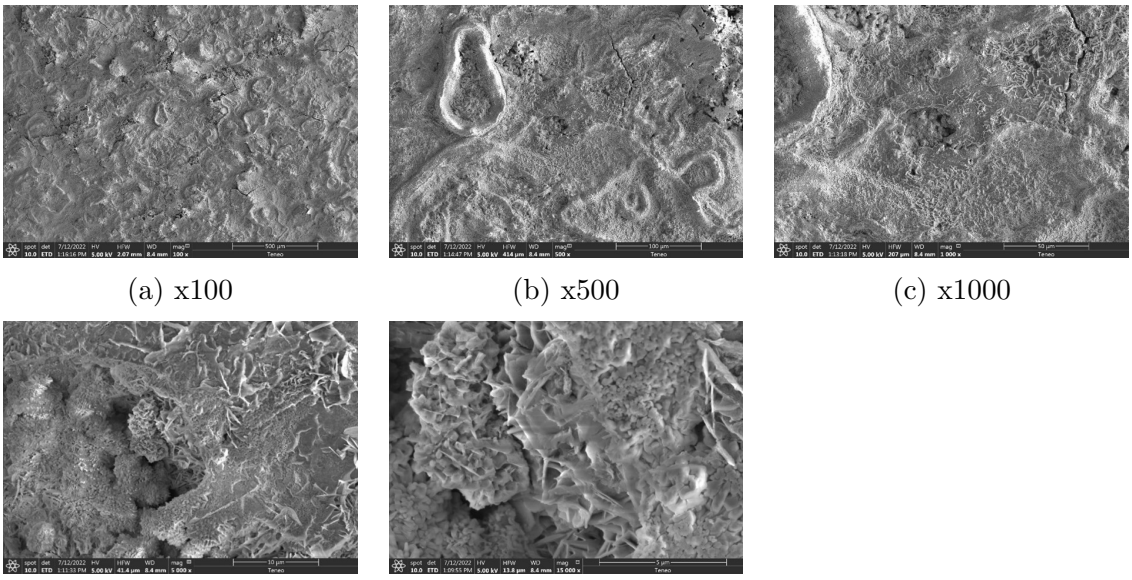

(a) x100 (b) x500 (c) x1000

(d) x5000 (e) x15000

Figure 62: Corrosion product on samples exposed to pH 3.5 H_2SO_4 18 days

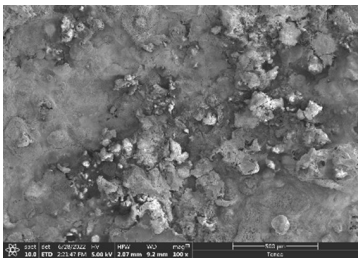

(a) x100

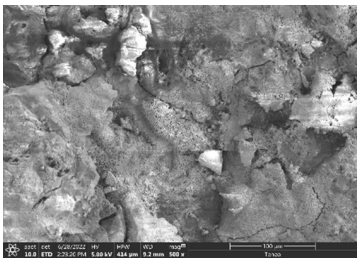

(b) x500

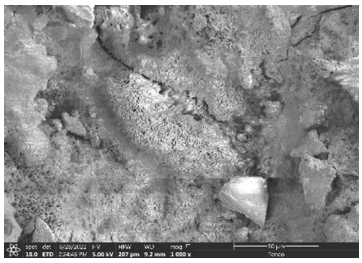

(c) x1000

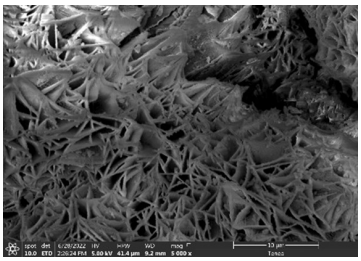

(d) x5000

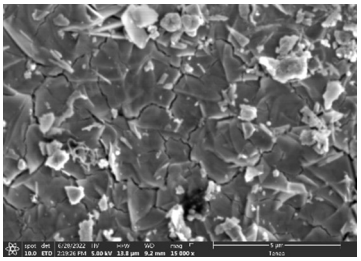

(e) x15000

Figure 63: Corrosion product on samples exposed to pH 7 0.1 M NaCl 6 days

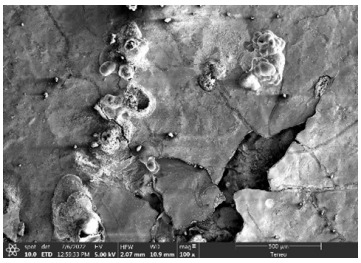

(a) x100

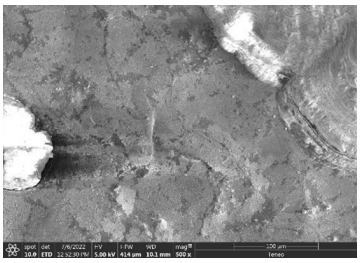

(b) x500

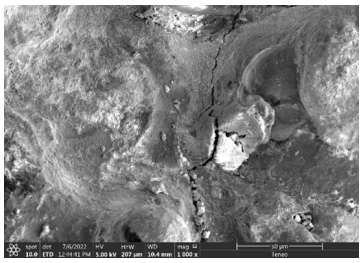

(c) x1000

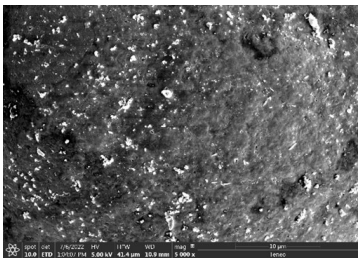

(d) x5000

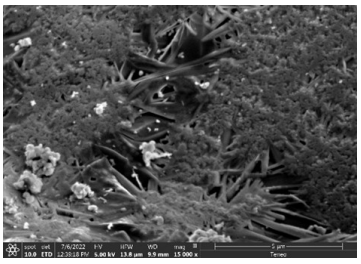

(e) x15000

Figure 64: Corrosion product on samples exposed to pH 7 0.1 M NaCl 12 days

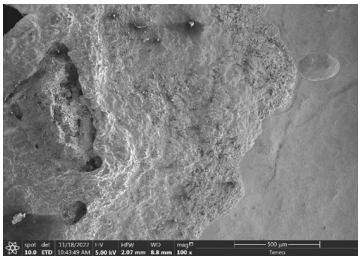

(a) x100

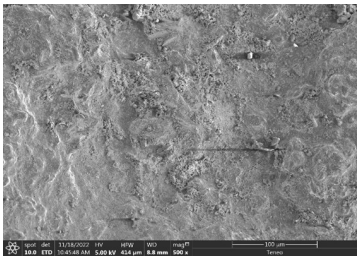

(b) x500

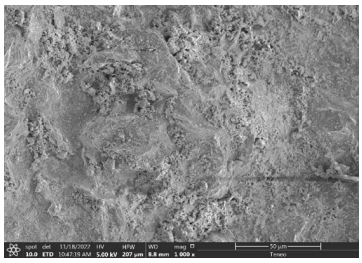

(c) x1000

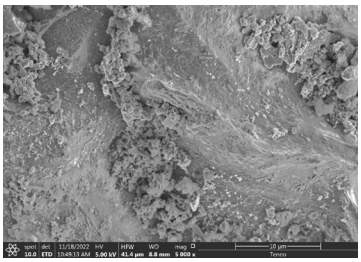

(d) x5000

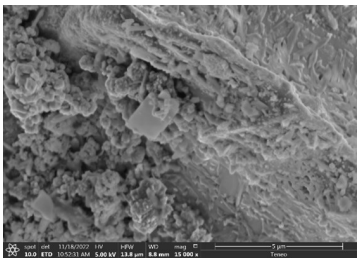

(e) x15000

Figure 65: Corrosion product on samples exposed to pH 7 0.6 M NaCl 9 days

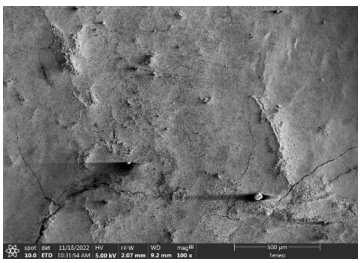

(a) x100

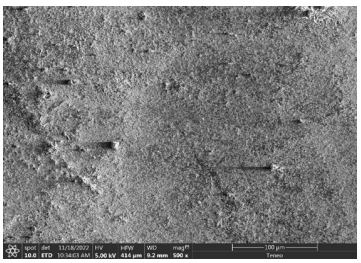

(b) x500

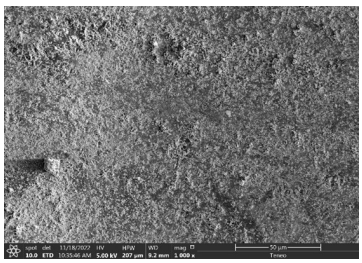

(c) x1000

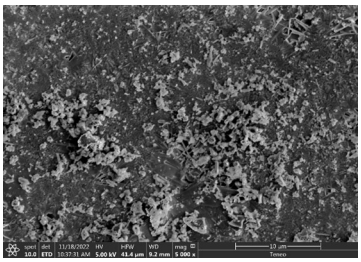

(d) x5000

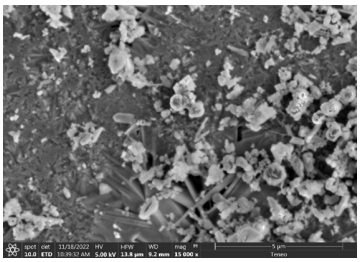

(e) x15000

Figure 66: Corrosion product on samples exposed to pH 7 0.6 M NaCl 15 days

References

[1] N. Mabho, K. Bergers, J. Flock, and U. Telgheder, "Determination of diffusible and total hydrogen concentration in coated and uncoated steel using melt and solid extraction techniques: Part i," *Talanta*, vol. 82, no. 4, pp. 1298–1305, 2010.

[2] K. Verbeken, "Analysing hydrogen in metals: bulk thermal desorption spectroscopy (tds) methods," in *Gaseous hydrogen embrittlement of materials in energy technologies*, pp. 27–55, Elsevier, 2012.

[3] T. Tsuru, Y. Huang, M. R. Ali, and A. Nishikata, "Hydrogen entry into steel during atmospheric corrosion process," *Corrosion science*, vol. 47, no. 10, pp. 2431–2440, 2005.

[4] L. Duprez, K. Verbeken, and M. Verhaege, "Effect of hydrogen on the mechanical properties of multiphase high strength steels," *Effect of hydrogen on materials*, pp. 62–69, 2009.

[5] M. Nagumo, K. Takai, and N. Okuda, "Nature of hydrogen trapping sites in steels induced by plastic deformation," *Journal of alloys and compounds*, vol. 293, pp. 310–316, 1999.

[6] E. Fallahmohammadi, F. Bolzoni, G. Fumagalli, G. Re, G. Benassi, and L. Lazzari, "Hydrogen diffusion into three metallurgical microstructures of a c–mn x65 and low alloy f22 sour service steel pipelines," *International Journal of Hydrogen Energy*, vol. 39, no. 25, pp. 13300–13313, 2014.

[7] R. Ma, S. Xiang, and X. Zhang, "Repairing irreversible hydrogen–induced damages using electric current pulse," *International Journal of Hydrogen Energy*, vol. 45, no. 33, pp. 16909–16917, 2020.

[8] H. Wipf *et al.*, *Hydrogen in metals III: properties and applications*, vol. 73. Springer, 1997.

[9] S. Dey, A. Mandhyan, S. Sondhi, and I. Chattoraj, "Hydrogen entry into pipeline steel under freely corroding conditions in two corroding media," *Corrosion Science*, vol. 48, no. 9, pp. 2676–2688, 2006.

[10] D. Rudomilova, T. Prošek, and G. Luckeneder, "Techniques for investigation of hydrogen embrittlement of advanced high strength steels," *Corrosion Reviews*, vol. 36, no. 5, pp. 413–434, 2018.

[11] U. Hadam and T. Zakroczymski, "Absorption of hydrogen in tensile strained iron and high-carbon steel studied by electrochemical permeation and desorption techniques," *International Journal of Hydrogen Energy*, vol. 34, no. 5, pp. 2449–2459, 2009.

[12] I. Maroef, D. Olson, M. Eberhart, and G. Edwards, "Hydrogen trapping in ferritic steel weld metal," *International Materials Reviews*, vol. 47, no. 4, pp. 191–223, 2002.

[13] I. Khader, D. Kürten, R. Raga, N. Winzer, and A. Kailer, "Modeling hydrogen diffusion in a tribological scenario: A failure analysis of a thrust bearing," *Wear*, vol. 438, p. 203054, 2019.

[14] K. FLOWERS, "Bearing repair provides valuable alternative to bearing replacement for heavy industries," *Iron & steel technology*, vol. 6, no. 6, pp. 85–89, 2009.

[15] R. Vegter, "Skf engineering research centre, houten, the netherlands," August 2022.

[16] T. A. Harris and M. N. Kotzalas, *Essential concepts of bearing technology*. CRC press, 2006.

[17] "239/560-b-k-mb-c3 fag." `https://www.abf.store/s/en/bearings/239-560-B-K-MB-C3-FAG/650936`, accessed May 9, 2023.

[18] T. A. Harris and M. N. Kotzalas, *Essential concepts of bearing technology*.

[19] J. F. Moulder, W. F. Stickle, P. E. Sobol, and K. D. Bomben, "Handbook of x-ray photoelectron spectroscopy: a reference book of standard spectra for identification and interpretation of xps data, 1992," *Google Scholar There is no corresponding record for this reference*, 2000.

[20] B. A. Szost, *Hydrogen trapping in bearing steels: mechanisms and alloy design*. PhD thesis, University of Cambridge, 2013.

[21] G. Pressouyre, "A classification of hydrogen traps in steel," *Metallurgical Transactions A*, vol. 10, pp. 1571–1573, 1979.

[22] A. Valor, F. Caleyo, L. Alfonso, D. Rivas, and J. Hallen, "Stochastic modeling of pitting corrosion: a new model for initiation and growth of multiple corrosion pits," *Corrosion science*, vol. 49, no. 2, pp. 559–579, 2007.

[23] G. Frankel and N. Sridhar, "Understanding localized corrosion," *Materials today*, vol. 11, no. 10, pp. 38–44, 2008.

[24] X. Zhang, W. Wu, H. Fu, and J. Li, "The effect of corrosion evolution on the stress corrosion cracking behavior of mooring chain steel," *Corrosion Science*, vol. 203, p. 110316, 2022.

[25] J. R. Galvele, "Transport processes and the mechanism of pitting of metals," *Journal of the Electrochemical Society*, vol. 123, no. 4, p. 464, 1976.

[26] M. Cerit, K. Genel, and S. Eksi, "Numerical investigation on stress concentration of corrosion pit," *Engineering failure analysis*, vol. 16, no. 7, pp. 2467–2472, 2009.

[27] Y. Hirose and T. Mura, "Crack branching behavior in stress corrosion cracking of high strength steel," *Engineering Fracture Mechanics*, vol. 34, no. 3, pp. 729–742, 1989.

[28] M. A. Stopher, P. Lang, E. Kozeschnik, and P. E. Rivera-Diaz-del Castillo, "Modelling hydrogen migration and trapping in steels," *Materials & Design*, vol. 106, pp. 205–215, 2016.

[29] F. J. López-Uruñuela, B. Fernández-Díaz, B. Pinedo, and J. Aguirrebeitia, "Early stages of subsurface crack and wec formation in 100cr6 bearing steel under rcf and hydrogen influence," *International Journal of Fatigue*, vol. 155, p. 106587, 2022.

[30] B. Evgeny, T. Hughes, and D. Eskin, "Effect of surface roughness on corrosion behaviour of low carbon steel in inhibited 4 m hydrochloric acid under laminar and turbulent flow conditions," *Corrosion Science*, vol. 103, pp. 196–205, 2016.

[31] M. Nagano, Y. Hayashi, N. Ohtani, M. Isshiki, and K. Igaki, "Diffusion of hydrogen and deuterium in high purity iron between 222 and 322 k," *Transactions of the Japan Institute of Metals*, vol. 22, no. 6, pp. 423–429, 1981.

[32] S. M. Charca, O. N. Uwakweh, and V. S. Agarwala, "Hydrogen transport conditions and effects in cathodically polarized af1410 steel," *Metallurgical and materials transactions A*, vol. 38, pp. 2389–2399, 2007.

[33] J. Venezuela, E. Gray, Q. Liu, Q. Zhou, C. Tapia-Bastidas, M. Zhang, and A. Atrens, "Equivalent hydrogen fugacity during electrochemical charging of some martensitic advanced high-strength steels," *Corrosion Science*, vol. 127, pp. 45–58, 2017.

[34] F. G. Wei and K. Tsuzaki, "Quantitative analysis on hydrogen trapping of tic particles in steel," *Metallurgical and Materials Transactions*, vol. 37, no. 2, p. 331, 2006.

[35] M. Morcillo, B. Chico, I. Díaz, H. Cano, and D. De la Fuente, "Atmospheric corrosion data of weathering steels. a review," *Corrosion Science*, vol. 77, pp. 6–24, 2013.

[36] R. Nishimura, D. Shiraishi, and Y. Maeda, "Hydrogen permeation and corrosion behavior of high strength steel mcm 430 in cyclic wet–dry so2 environment," *Corrosion science*, vol. 46, no. 1, pp. 225–243, 2004.

[37] M. A. Azam, M. F. Ibrahim, and M. Zaimi, "Corrosion analysis of carbon steel pipeline: effect of different sulfuric acid concentrations," in *Applied Mechanics and Materials*, vol. 699, pp. 215–220, Trans Tech Publ, 2015.

[38] X. Wen, P. Bai, B. Luo, S. Zheng, and C. Chen, "Review of recent progress in the study of corrosion products of steels in a hydrogen sulphide environment," *Corrosion Science*, vol. 139, pp. 124–140, 2018.

[39] Z. Panossian, N. L. de Almeida, R. M. F. de Sousa, G. de Souza Pimenta, and L. B. S. Marques, "Corrosion of carbon steel pipes and tanks by concentrated sulfuric acid: a review," *Corrosion Science*, vol. 58, pp. 1–11, 2012.

[40] S. Dean Jr and G. Grab, "Corrosion of carbon steel tanks in concentrated sulfuric acid service," *Materials performance*, vol. 25, no. 7, pp. 48–52, 1986.

[41] W. P. Banks and J. D. Sudbury, "Anodic protection of carbon steel in sulfuric acid," *Corrosion*, vol. 19, no. 9, pp. 300t–307t, 1963.

[42] T. Dara, "Evaluation of atmospheric corrosion in steels for corrosion mapping in asia."," 2017.

[43] E. J. Reardon, "Anaerobic corrosion of granular iron: Measurement and interpretation of hydrogen evolution rates," *Environmental science & technology*, vol. 29, no. 12, pp. 2936–2945, 1995.

[44] Y. Wang, G. Cheng, W. Wu, Q. Qiao, Y. Li, and X. Li, "Effect of ph and chloride on the micro-mechanism of pitting corrosion for high strength pipeline steel in aerated nacl solutions," *Applied Surface Science*, vol. 349, pp. 746–756, 2015.

[45] J. Calero, J. Alcántara, B. Chico, I. Díaz, J. Simancas, D. de la Fuente, and M. Morcillo, "Wet/dry accelerated laboratory test to simulate the formation of multilayered rust on carbon steel in marine atmospheres," *Corrosion Engineering, Science and Technology*, vol. 52, no. 3, pp. 178–187, 2017.

[46] P. Refait and J.-M. Génin, "The oxidation of ferrous hydroxide in chloride-containing aqueous media and pourbaix diagrams of green rust one," *Corrosion science*, vol. 34, no. 5, pp. 797–819, 1993.

[47] D.-h. Xia, S.-z. Song, J.-h. Wang, H.-c. BI, Y.-x. Jiang, and Z.-w. Han, "Corrosion behavior of tinplate in nacl solution," *Transactions of nonferrous metals society of China*, vol. 22, no. 3, pp. 717–724, 2012.

[48] F. Perez, C. Barrero, A. H. Walker, K. Garcia, and K. Nomura, "Effects of chloride concentration, immersion time and steel composition on the spinel phase formation," *Materials Chemistry and Physics*, vol. 117, no. 1, pp. 214–223, 2009.

[49] J. Jia, X. Cheng, X. Yang, X. Li, and W. Li, "A study for corrosion behavior of a new-type weathering steel used in harsh marine environment," *Construction and Building Materials*, vol. 259, p. 119760, 2020.

[50] R. Pascual Marqui, "Influencia de la concentración de ion cloruro sobre la corrosión atmosférica de un acero al carbono bajo capa de fase de humedad. rev," *Corros. Prot*, pp. 37–40, 1980.

[51] C. Barrero, A. Morales, J. Restrepo, G. Pérez, J. Tobón, J. Mazo-Zuluaga, F. Jaramillo, D. Escobar, C. Arroyave, R. Vandenberghe, *et al.*, "Synthesis of magnetite in presence of cu 2+ or cr 3+," *Hyperfine interactions*, vol. 134, pp. 141–152, 2001.

[52] M. Kimura, T. Suzuki, G. Shigesato, H. Kihira, and S. Suzuki, "Characterization of nanostructure of rusts formed on weathering steel," *ISIJ international*, vol. 42, no. 12, pp. 1534–1540, 2002.